

1 Changing Characteristics of Runoff and Freshwater
2 Export From Watersheds Draining Northern
3 Alaska

4 Michael A. Rawlins¹, Lei Cai², Svetlana L. Stuefer³, and Dmitry
5 Nicolsky⁴

6 ¹Department of Geosciences, University of Massachusetts, Amherst,
7 MA 01003, USA

8 ²International Arctic Research Center, University of Alaska Fairbanks,
9 Fairbanks, AK 99775

10 ³Civil and Environmental Engineering, College of Engineering and
11 Mines, University of Alaska Fairbanks, Fairbanks, AK 99775 USA

12 ⁴Geophysical Institute, University of Alaska Fairbanks, Fairbanks, AK
13 99775, USA

14 Corresponding author: Michael A. Rawlins <rawlins@geo.umass.edu>

15 **Abstract**

16 The quantity and quality of river discharge in arctic regions is influenced
17 by many processes including climate, watershed attributes and, increasingly,
18 hydrological cycle intensification and permafrost thaw. We used a hydrological
19 model to quantify baseline conditions and investigate the changing character
20 of hydrological elements for Arctic watersheds between Point Barrow and
21 just west of Mackenzie River over the period 1981–2010. ~~The region annually~~
22 ~~exports 28.1~~ A synthesis of measurements and model simulations shows that
23 the region exports 31.9 km³ yr⁻¹ of freshwater via river discharge, with 51.9%
24 (14.6–57.7% (18.4 km³ yr⁻¹)) coming collectively from the Colville, Kuparuk,
25 and Sagavanirktok rivers. ~~Our results~~ The simulations point to significant (p <

26 0.05) increases (134–212% of average) in cold season discharge (CSD) for sev-
27 eral large North Slope rivers including the Colville and Kuparuk, and for the
28 region as a whole. A significant increase in the proportion of subsurface runoff
29 to total runoff is noted for the region and for 24 of the 42 study basins, with
30 the change most prevalent across the northern foothills of the Brooks Range.
31 Relatively large increases in simulated active-layer thickness (ALT) suggest a
32 physical connection between warming climate, permafrost degradation, and in-
33 creasing subsurface flow to streams and rivers. A decline in terrestrial water
34 storage (TWS) is attributed to losses in soil ice that outweigh gains in soil liquid
35 water storage. Over the 30 yr period the timing of peak spring (freshet) dis-
36 charge shifts earlier by 4.5 days, though the time trend is only marginally ($p =$
37 0.1) significant. These changing characteristics of Arctic rivers have important
38 implications for water, carbon, and nutrient cycling in coastal environments.

39 KEYWORDS: Arctic; runoff; river discharge; permafrost; subsurface flow

40 1 Introduction

41 The arctic water cycle is central to a range of climatic processes and to the
42 transfer of carbon, energy, and ~~a host of other constituents~~ other materials from the
43 land mass to coastal waters of the Arctic Ocean. Freshwater export to the Arctic
44 Ocean is high relative to the ocean’s area (Shiklomanov et al., 2000), and dominated
45 by river discharge (Serreze et al., 2006), which serves as a conveyance for carbon and
46 heat across the land-ocean boundary. Syntheses of data and models have advanced
47 understanding of key linkages and feedbacks in the Arctic system (Francis et al.,
48 2009), mean freshwater budgets across the land, atmosphere and ocean domains
49 (Serreze et al., 2006), and time trends in observations and model estimates over the
50 latter decades of the 20th century (Rawlins et al., 2010).

51 A warming climate is expected to lead to intensification of the hydrological cycle,
52 including increases in net precipitation (P) at high latitudes. ~~Evidence pointing to~~
53 ~~Arctic hydrological cycle~~, and evidence of broad-scale intensification is emerging
54 (Peterson et al., 2002, 2006; Rawlins et al., 2010; Zhang et al., 2013; Bring et al.,
55 2016). A more vigorous water cycle is related ~~both to in part to both~~ the amount of
56 moisture air can hold and changes in atmospheric dynamics. Shorter ice duration on
57 lakes and longer seasons for evaporation are also manifestations of warming on the
58 Arctic hydrological cycle. Much of the increase in net P is expected to occur during
59 winter (Kattsov et al., 2007), potentially through intensified local surface evaporation
60 driven by retreating winter sea ice, and enhanced moisture inflow from lower latitudes
61 (Zhang et al., 2013; Bintanja and Selten, 2014). An increase in river discharge from

62 Eurasia to the Arctic Ocean was noted in simulations with the HadCM3 general
63 circulation model (Wu et al., 2005), illustrating the potential for increased winter net
64 P to influence freshwater export. Positive trends in column-integrated precipitable
65 water over the region north of 70°N, linked to positive anomalies in air and sea surface
66 temperature and negative anomalies in end-of-summer sea ice extent (Serreze et al.,
67 2012), support the future model projections. Rivers form a primary conduit for
68 transferring terrestrial materials to the coastal ocean, and these materials exert a
69 strong influence on marine ecosystems and carbon processing.

70 Permafrost warming and degradation has been observed over parts of Alaska,
71 Russia, and Canada (Brown and Romanovsky, 2008; Romanovsky et al., 2010; Smith
72 et al., 2010). In one study permafrost area is projected to decrease by more than
73 40%, assuming climate stabilization at 2°C above pre-industrial (Chadburn et al.,
74 2017). Warming and permafrost degradation is expected to cause a shift in arctic
75 environments from a surface water-dominated system to a groundwater-dominated
76 system (Frey and McClelland, 2009; Bring et al., 2016). There is increasing evi-
77 dence of impacts of permafrost degradation on biogeochemical cycles on land and
78 in aquatic systems. Recent reported increases in baseflow in arctic rivers are sug-
79 gestive of increased hydrological ~~conductivity~~ connectivity due to permafrost thaw
80 (~~Walvoord and Striegl, 2007; Bense et al., 2009; St. Jacques and Sauchyn, 2009~~) (Walvoord and Striegl, 2007; Bense et al., 2009; St. Jacques and Sauchyn, 2009)
81 Groundwater processes have a dominant role in controlling carbon export from the
82 land to streams in permafrost terrain (Frey and McClelland, 2009; Neilson et al.,
83 2018). In areas where much of the landscape is defined by the absence of permafrost, runoff generation processes can be much different from areas where permafrost is nearly continuous. Dissolved organic matter (DOM) transported by Arctic rivers
84 contain geochemical signatures of the watersheds they drain, reflecting their unique
85 characteristics (Kaiser et al., 2017). Changes in landscape characteristics and water
86 flow paths as a result of climatic warming and associated active layer thickening
87 have the potential to alter aquatic and riverine biogeochemical fluxes (Frey and Mc-
88 Clelland, 2009; Wrona et al., 2016; Wickland et al., 2018). Increased flow through
89 mineral soils has been linked to decreases in DOC export from the Yukon River
90 over recent decades (Striegl et al., 2005). In contrast, areas with deep peat deposits
91 that experience thaw may see increasing DOC mobilization and export as permafrost
92 degrades (Frey and Smith, 2005).

95 This study presents baseline freshwater flux estimates and examines elements of
96 the hydrological cycle across the North Slope over the period 1981–2010. We use mea-
97 sured data to assess model performance and combine with the simulated estimates
98 to quantify freshwater export from the region. We then ~~leverage the modeling~~
99 ~~framework to investigate signs of change~~ use the data and model simulations to

100 investigate time changes in runoff and river discharge, the proportion of groundwa-
101 ter runoff, terrestrial water storage, and the timing of peak daily discharge. Salient
102 results in the context of arctic change and directions for future research are discussed.

103 2 Study Area, Data and Modeling

104 ~~Our~~ The study focuses on the North Slope of Alaska and ~~far~~-NW Canada, parti-
105 tioned by the region’s river basins that drain to the Beaufort Sea ~~and Arctic Ocean~~.
106 ~~In the text,~~ (Figure 1). Hereafter we refer to ~~the entire study area this region~~ as
107 the “North Slope”. ~~Model input and output fields are resolved at a daily time step.~~
108 The grid is based on the Northern Hemisphere EASE-Grid (Brodzik and Knowles,
109 2002), with a horizontal resolution of 25 km for each grid cell. The ~~area draining the~~
110 ~~North Slope model domain~~ contains 312 grid cells (total area = 196,060 km²) ~~across~~
111 that define the North Slope drainage of northern Alaska and ~~extreme northwest NW~~
112 Canada. It is defined by the ~~watersheds drainage basins of rivers~~ (42 ~~in total~~) ~~of~~
113 ~~rivers total~~, Table S1) with an outlet along the coast from just west of the Mackenzie
114 River to Utqiavik (formerly Barrow) to the west. Hydrologic modeling was per-
115 formed for the North Slope domain encompassing the 42 watersheds. Many North
116 Slope rivers are oriented roughly north-south. ~~The study area, and the region~~ is
117 underlain by continuous permafrost, approximately 250–300 m thick in the Brooks
118 Range and, locally, up to nearly 400 m thick near the coast (Jorgenson et al., 2008).

119 2.1 Observational data

120 Observational data used in this study include time series of daily river discharge,
121 end-of-winter snow water equivalent (SWE), and seasonal maximum active-layer
122 thickness (ALT). Historical river discharge data was retrieved from the USGS for the
123 Kuparuk River (~~station~~ <http://waterdata.usgs.gov/nwis/uv?15896000>) ~~was retrieved~~
124 ~~from the USGS at http~~ and Colville River ([https://waterdata.usgs.gov/ak/nwis/uv?15896000-](https://waterdata.usgs.gov/ak/nwis/uv?15896000-/?site_no=15875000)
125 [/?site_no=15875000](https://waterdata.usgs.gov/ak/nwis/uv?15896000-/?site_no=15875000)). Model simulated SWE is evaluated against average end-of-winter
126 SWE from measurements across the Kuparuk River watershed. The measurements
127 from 2000 to 2011 were taken at multiple locations distributed from the Brooks
128 Range to the Beaufort Sea coast to better capture macro-scale SWE variability
129 (Stuefer et al., 2013).

130 Simulated ALT from the PWBM (section 2.3) is compared with estimates from
131 a ~~related~~ high-resolution 1-D heat conduction model (developed by the University of
132 Alaska’s Geophysical Institute Permafrost Laboratory, hereafter referred to as GIPL)
133 that incorporated data on ecosystem type and was validated against measured CALM

134 network ALTs (Nicolson et al., 2017). ~~Model simulated SWE is evaluated against~~
135 ~~average values from 12 years of SWE observations collected across a 200×300 km~~
136 ~~domain that includes the Kuparuk River watershed from the Brooks Range to the~~
137 ~~Beaufort Sea coast (Stuefer et al., 2013).~~

138 2.2 Reanalysis data

139 Gridded fields of daily surface (2 m) air temperature, precipitation (P), and wind
140 speed are used as model forcings. Obtaining accurate temporally varying P estimates
141 at daily resolution is particularly challenging in arctic environments. Gauge undercatch
142 of solid P is common, the gauge network is sparse and the number of stations at higher
143 elevation is insufficient (Yang et al., 1998, 2005; Kane and Stuefer, 2015). In this
144 study model meteorological forcings are drawn from the Modern-Era Retrospective
145 Analysis for Research and Applications (MERRA; Rienecker et al. (2011)). In a
146 recent intercomparison of P estimates over the Arctic Ocean and its peripheral seas,
147 three reanalyses— ERA-Interim (Dee et al. (2011)), MERRA, and NCEP R2 (Kistler
148 et al. (2001))— produce realistic magnitudes and temporal agreement with observed
149 P events, while two products (MERRA, version 2 (MERRA-2), and CFSR) show
150 large, implausible magnitudes in P events (Boisvert et al., 2018). Given a modest
151 low bias in monthly P across the North Slope in MERRA, we derived a new bias
152 corrected daily P time series by scaling the MERRA values by a factor defined using
153 monthly long-term mean P (1981–2010) from MERRA, ERA-Interim, and a data set
154 that blends simulations from ERA-Interim and the Polar WRF (Cai et al., 2018).
155 Those three data sets exhibit a similar spatial pattern in annual P across the region.
156 Annual P generally ranges from as low as 200 mm yr⁻¹ near the coast to over 400
157 mm yr⁻¹ over the foothills of the Brooks Range. At each grid cell, the offset ratio
158 was defined as average P from the 3 data sets divided by the MERRA P amount.
159 The derived daily P (hereafter MERRA*) was then calculated as the daily MERRA
160 P amount multiplied by the offset ratio.

161 2.3 Hydrological modeling

162 The regional hydrology is characterized by water fluxes and storages expressed
163 in simulations using a spatially-distributed numerical model. Referenced previously
164 as the Pan-Arctic Water Balance Model (PWBM), the numerical framework en-
165 compasses all major elements of the water cycle, including snow storage, sublima-
166 tion, transpiration, and surface evaporation (Rawlins et al., 2003, 2013). ~~It is run~~
167 Model input and output fields are resolved at a daily time step. The simulations

168 are commonly performed at an implicit daily time step ~~and is~~, typically forced with
169 meteorological data. The PWBM has been used to investigate causes behind the
170 record Eurasian discharge in 2007 (Rawlins et al., 2009); to corroborate remote sens-
171 ing estimates of surface water dynamics (Schroeder et al., 2010); and to quantify
172 present and future water cycle changes in the area of Nome, Alaska (Clilverd et al.,
173 2011). In a comparison against observed river discharge, PWBM-simulated SWE
174 fields compared favorably (Rawlins et al., 2007). Soil temperature ~~dynamics are~~
175 ~~simulated through a~~ are simulated dynamically are through an embedded 1-D non-
176 linear heat conduction ~~model-sub-model~~ with phase change (Rawlins et al., 2013;
177 Nicolsky et al., 2017). PWBM includes a multi-layer snow model that accounts for
178 wind compaction, change in density due to fresh snowfall, and depth hoar develop-
179 ment with time. Runoff is the sum total of surface (overland) and subsurface flow
180 each day. Subsurface runoff occurs when the amount of water in a soil layer exceeds
181 field capacity.

182 The model is well suited for application across the North Slope region. Active-
183 layer thickness (ALT) simulated using the PWBM ~~soil-submodel~~ was found to be
184 more similar to in situ observations and airborne radar retrievals in continuous per-
185 mafrost areas than in lower permafrost probability areas (Yi et al., 2018). The influ-
186 ence of snow cover and soil thermal dynamics on the seasonal and spatial variability
187 in soil CO₂ respiration ~~was~~ has been quantified by coupling PWBM to a dynamic
188 soil carbon model (Yi et al., 2013, 2015). A key model attribute is its ability to dy-
189 namically simulate the direct influence the snowpack exerts on soil temperature (Yi
190 et al., 2019), with deeper snowpacks promoting warmer soils and associated effects,
191 such as enhancement of soil decomposition and respiration from deeper (≥ 0.5 m)
192 soil layers (Yi et al., 2015). Detailed descriptions of the PWBM can be found in
193 Rawlins et al. (2003, 2013); Yi et al. (2015, 2019) and Appendices within.

194 In this study we applied an updated version of the model, and given its detailed
195 representation of soil freeze-thaw processes, rename it the “Permafrost Water Bal-
196 ance Model” (hereafter PWBM v3). ~~Modifications~~ Recent modifications involved
197 the incorporation of new data and parametrizations for surface fractional open wa-
198 ter (f_w) cover, soil carbon content, and transient ponded surface evaporation and
199 runoff. Updates to the spatial estimates of f_w were ~~taken~~ drawn from a product
200 derived from brightness temperature (T_b) retrievals from the Advanced Microwave
201 Scanning Radiometer for EOS (AMSR-E) (Du et al., 2017) to parameterize the grid
202 cell fraction of open water (annual average) across the model domain. Properties of
203 near surface organic-rich soils strongly control hydrological and thermal dynamics
204 in the seasonally thawed active layer. We used soil organic carbon (SOC) estimates
205 from version 2.2 of the Northern Circumpolar Soil Carbon Database (NCSCD), a

206 digital soil map database linked to extensive field-based SOC storage data (Hugelius
 207 et al., 2014). The database contains SOC stocks for the upper 0–1 m and for deeper
 208 soils from 1–2 and 2–3 m depth. In the updated PWBm v3 the sum total of SOC in
 209 the upper 3 m was used to derive the organic layer thickness as described in Rawlins
 210 et al. (2013). The resulting spatially varying parameterizations of soil carbon pro-
 211 files (% of volume) with depth over the domain (Figure S1**a**) influence soil thermal
 212 properties and hydrological storages and fluxes. ~~The maps show broad agreement~~
 213 Broad agreement exists in the spatial pattern of the independent soil ~~texture and~~
 214 ~~soil carbon datasets~~ carbon and soil texture datasets (Figure S1**a,b**). Sandy soils
 215 and soil carbon thicknesses under 20 cm occur over the Brooks Range, and relatively
 216 higher soil carbon thicknesses and loam soils are present across the tundra to the
 217 north. ~~Following initial assessments~~ Based on analysis of initial model simulations
 218 we increased soil carbon amounts by 10% in areas (24 grid cells) of sandy soils and
 219 reassigned ~~24 grid cells~~ the texture to loam, ~~to be making the parameterizations~~
 220 more consistent with soil textures inferred from ~~the~~ high-resolution ALT mapping
 221 via using the GIPL model that incorporated data on ecosystem type (Nicolosky et al.,
 222 2017).

223 Model calibration was performed to adapt the model and optimize its performances
 224 in simulating the water cycle across the study domain, and involved the surface
 225 transient storage pool and river flow velocity. Transient surface storage consists
 226 of water connected to the surface flow that is delayed in its transport to stream
 227 networks. Parameters controlling evaporation and runoff fluxes from ~~transient surface~~
 228 ~~storages~~ surface storage were modified to better account for delays in water reaching
 229 stream channels. Defining ~~$E_i, R_i,$ and S_i~~ $E_i, R_i,$ and S_i to represent evaporation (or
 230 evapotranspiration)(mm day⁻¹), runoff (mm day⁻¹, and storage (mm) in soil layer
 231 ~~i~~ , respectively, then ~~E_0, R_0, S_0~~ E_0, R_0, S_0 are evaporation, runoff, and storage from
 232 the model surface layer, ~~$R_0 = S_0 * f$~~ $R_0 = S_0 * f$ (mm day⁻¹). In the updated model
 233 $f = 0.40$, reduced from the prior value of 0.75. Evaporation from surface storage is
 234 ~~$E_0 = S_0 * g$~~ $E_0 = S_0 * g$, with g now reduced to 1/3 of the potential ET rate.

235 Model estimated runoff routed through a simulated topological network (STN)
 236 (Vörösmarty et al., 2000) is expressed as river discharge (volume flux) at the coastal
 237 outlets of 42 individual watersheds draining from Point Barrow to just west of the
 238 Mackenzie River delta. A simple linear routing model is used given the relatively
 239 short travel times through the North Slope basins. Water transferred to the down-
 240 stream grid ~~(or ocean/lagoon)~~ is or exported off the coast is

$$\underline{Q_{out} = \frac{v}{d} S} \underline{Q_{out} = \frac{v}{d} S} \quad (1)$$

241 where Q_{out} ($m^3 s^{-1}$) is flow downstream, v is flow velocity ($m s^{-1}$), d is the
242 distance between grid cells (m), and S is volume of river water (m^3). Miller et al.
243 (1994) suggested a global average of $v = 0.35 m s^{-1}$. Given the relatively flat to-
244 pography over much of the domain we set effective velocity at $v = 0.175$. Hereafter
245 R represents runoff expressed in unit depth, and Q represents river discharge volume
246 flow estimated through the routing model.

247 The model-PWBM is run in a 50 year spinup over year 1980 prior to the transient
248 time series simulation to stabilize soil temperature and water storage pools. This
249 spinup is followed by a 30 year transient simulation over the period 1981–2010, the
250 focus of our analysis.

251 ~~Statistical significance of a time trend in runoff or river discharge is assessed~~
252 ~~Assessment of several model simulated quantities is made using average error and~~
253 ~~correlation. Model evaluation metrics based on squared values like the root mean~~
254 ~~square error (RMSE) are known to be biased and highly sensitive to outliers (Willmott and Matsuura, 2002).~~
255 ~~Statistical significance is calculated~~ using the Mann-Kendall test statistic (Hamed
256 and Rao, 1998; Yue et al., 2002), with a 95% confidence level ($p < 0.05$) desig-
257 nated as statistically significant. ~~A Time changes are estimated with a~~ General Lin-
258 ear Model (GLM) ~~is assumed for other analyzed quantities. We apply the modified~~
259 ~~Mann-Kendall test (Hamed and Rao, 1998) for terrestrial water storage (TWS) and~~
260 ~~its component storages of snow (water equivalent), soil liquid water and ice amounts.~~
261 A one or a two-sided test is applied depending on whether the direction of change
262 is assumed. For example, we posit null hypotheses that the region is experiencing
263 increasing cold season discharge as a result of ALT increase. ~~Percent change over~~
264 ~~time is estimated using the GLM linear least squares slope and the climatological~~
265 ~~average for the time series examined.~~

266 3 Results Model Validation

267 3.1 Active layer thickness

268 Simulated maximum seasonal ALT derived from daily soil temperatures in the
269 updated PWBM v3 model ~~run using the MERRA simulation with meteorological~~
270 ~~forcing from MERRA reanalysis~~ (bias corrected MERRA* P) ~~display is evaluated~~
271 ~~alongside ALT predicted from the GIPL model. Area averaged ALT from PWBM and~~
272 ~~GIPL is 53.5 and 55.2 cm respectively, a difference of $\sim 3\%$ (Figure S2, Table 1), and~~
273 ~~smallest difference among average ALT derived from soil temperatures in simulations~~
274 ~~using alternate meteorological forcings. Simulated ALT exhibits~~ the expected north-
275 south gradient which reflects the gradient in summer (and annual) air temperature

276 ~~.- The pattern is also evident in ALT predicted from the GIPL, with agreement~~
277 ~~(Figure S3). Agreement in ALT between PWBM (MERRA*) and GIPL is strongest~~
278 ~~in coastal areas. The fields differ estimates differ most~~ near the center of the domain
279 where the PWBM produces relatively ~~lower smaller~~ ALT compared to GIPL. ~~Area~~
280 ~~averaged ALT from PWBM and GIPL is 53.5 and 55.2 cm respectively, a difference of~~
281 ~~~3% (Table 1).~~ The differences increase toward the extremes of each field, pointing
282 to ~~larger higher~~ spatial variability in the PWBM simulations (Figure S2). ALT from
283 simulations with the default MERRA P forcing are shallower and less in agreement
284 with the GIPL data.

285 3.2 Snow water equivalent

286 ~~Within the Kuparuk In the Kuparuk River~~ basin maximum end of season SWE
287 typically occurs near the end of April. ~~Model simulated (PWBM v3) Simulated~~
288 end of season SWE each year is calculated as the average of daily values from April
289 24 to May 7, also averaged across all basin ~~grids. The model grid cells. Average~~
290 ~~simulated~~ SWE largely tracks the interannual variations in measured end of season
291 SWE over the period 2000–2010, with an average difference of 5.3 mm or 4.8% of
292 the average (109.7 mm) from the field measurements (Figure S4). The Pearson
293 correlation ~~efficient coefficient~~ is $r = 0.78$, with the relationship significant at $p <$
294 0.01 (Figure S5).

295 3.3 Runoff and river discharge

296 3.3.1 Spring freshet

297 Modeled ~~spring freshet~~ runoff (R) ~~from the simulation forced with MERRA*~~
298 evaluated against observed R for the ~~Kuparuk River watershed Colville and Kuparuk~~
299 ~~River watersheds~~. USGS measurements for the Kuparuk River at Deadhorse over
300 the period 1981–2010 show that an average of 98.3 mm of runoff (R) is exported as
301 discharge during the spring freshet, which we calculate as R occurring from day of
302 year (DOY) 100 to ~~180. R is the unit depth of discharge over a given time interval,~~
303 ~~and distributed over a contributing watershed. Modeled freshet R calculated from~~
304 ~~the simulation forced with MERRA* leads the observed freshet R by approximately~~
305 ~~10 days. This despite a relatively slow model river flow velocity ($v = 0.175 \text{ m}^3 \text{ s}^{-1}$)~~
306 ~~(Figure 2, 3b).~~ Simulated R over the freshet period ~~is totals~~ 98.0 mm. Simulated May
307 R exceeds observed R by 29 mm month⁻¹, while simulated June R is 29 mm month⁻¹
308 lower than observed R (Figure 2), resulting in the relatively small error (percent
309 difference +0.3%) for total R over the freshet period. Simulated R closely tracks

310 observed R in other months of the year with flow (Figure 2). For the Colville River,
311 the available data beginning in late May show that the total volume simulated over
312 the spring freshet is well captured, with average error of 10% (Figure 3a). Simulated
313 R is underestimated in summer. The timing of simulated maximum daily Q closely
314 matches the timing based on the measured data (Figure 3a). For the Kugaruk River
315 simulated discharge leads observed discharge by approximately one week (-7.8 days,
316 Figure 3b). For this region the flow routing sub-model is relatively insensitive to the
317 specified flow velocity. Two sensitivity simulations using a velocity 33% lower and
318 33% higher than the default velocity ($v = 0.175 \text{ m}^3 \text{ s}^{-1}$) resulted in errors of -5.4
319 and -9.0 days respectively. Many of the rivers in this region are shorter than the
320 Kugaruk, so travel times are relatively brief.

321 **3.3.2 Annual runoff and freshwater export**

322 **3.3.2 Annual runoff**

323 Annual total P over the Kugaruk Basin ranges from 182 mm yr^{-1} (2007) to 433
324 mm yr^{-1} (2003) with no significant trend over the 30 year period (Figure 4). For
325 the Kugaruk River annual total R as the long-term (30 yr) average from USGS
326 observations and from the model simulation are 144 and 134 mm yr^{-1} , respectively
327 (percent difference = -6.8%). There is no significant trend in observed or simulated
328 annual R over the 30 yr period. Simulated annual R (Figure 4). Annual R from the
329 simulation is correlated with observed annual R (Pearson correlation $r = 0.74$, $p <$
330 0.001), with average error of $+3.1 \text{ mm yr}^{-1}$ (Figure S6). Observed R varies from
331 75 – 238 mm yr^{-1} , while simulated R is more conservative, extending over a range
332 from 90 – 200 mm yr^{-1} . In other words, the model tends to overestimate R in years
333 with low annual flow, and vice versa when observations are high and underestimate R
334 in years with low observed flow. For measured R partitioned at: $R < 100 \text{ mm yr}^{-1}$,
335 $100 \leq R \leq 200 \text{ mm yr}^{-1}$, and $R > 200 \text{ mm yr}^{-1}$, average errors are $+24.5$, -1.8 , and
336 -52.2 mm yr^{-1} , respectively. It is notable that in both 1996 and 2003, annual R
337 is higher in the year following a peak (within a several year span) in annual P. This
338 lag highlights the role that antecedent storage plays in the region's river discharge
339 regimes, and is consistent with previous research (Bowling et al., 2003; Stuefer et al.,
340 2017).

341 4 Baseline Hydrology and Assessment of Changes

342 4.1 Annual precipitation and river discharge

343 For the period 1981–2010 annual total P averaged across the North Slope drainage
344 basin ranged from 195 mm yr⁻¹ (1990) to 383 mm yr⁻¹ (2003) based on the adjusted
345 MERRA* P data. Annual total P over the Kuparuk Basin varied from 182 mm
346 yr⁻¹ (2007) to 433 mm yr⁻¹ (2003) (Figure 4). There is no significant trend in
347 observed or simulated annual P or R for the Kuparuk (Figure 4) or any other river
348 over the 30 yr period. Much higher annual runoff has been documented for the
349 Kuparuk River in 2013, 2014, and 2015 (Stuefer et al., 2017). The spatial pattern
350 in annual R (Figure 5a) reflects a similar gradient expressed in annual P from the
351 coast southward into the Brooks Range, as R in this region is largely controlled by
352 ~~P and snow accumulation variations across the region.~~ Annual R averages over 250
353 mm yr⁻¹ across parts of the Brooks Range, while coastal areas average under ~~50–100~~
354 mm yr⁻¹.

355 ~~In the modeling framework simulated~~ Simulated R is routed ~~along the gridded~~
356 ~~river network through the STN~~ and expressed as a volume flux of river discharge
357 (Q) at the Beaufort Sea coast. ~~For the period~~ There is a notable absence of routine
358 ~~monitoring of Q at river outlets near the coast.~~ The Colville, Kuparuk, and Sagavanirktok
359 Rivers are the three largest gauged North Slope rivers and occupy 46.2% of the study
360 domain. Measurements for the Kuparuk River at Deadhorse are year round since
361 the 1970s and capture flow from most of the basin. Data for the Colville at Umiat
362 are available from late May until early October since 2002, but Q from just 56%
363 of the full basin area flows past the gauge location. Data for the Sagavanirktok at
364 Pump Station 3 are available from June through September since 1995. This gauge
365 site is located far from the coast and captures Q from only 30% of the basin. Given
366 these constraints we estimate baseline Q exports using the observed data for the
367 Kuparuk River, a composite of measured data and model simulation for subbasins
368 of the Colville, and simulated Q for the remainder of the study domain.

369 Annual Q (1981–2010, ~~annual~~) for the Kuparuk River based on the USGS
370 observations is 1.4 km³ yr⁻¹ (144 mm yr⁻¹) (Table 2). The model simulated Q of
371 1.3 km³ yr⁻¹ closely aligns with the observations and matches the 1.3 km³ yr⁻¹ for
372 2000–2007 reported by McClelland et al. (2014) based on model simulations using
373 Catchment Based Land Surface Model (CLSM). We leverage the measured data for
374 the Colville River at Umiat (36,447 km²) to estimate total Q for the ~~Colville~~entire
375 ~~(60, Kuparuk, and Sagavanirktok rivers combined averages 14.57–095 km²)~~ Colville
376 River basin. A data-model composite for the subbasin defined by the gauge at Umiat

377 (area = 36,447 km²) is calculated from the daily averages using measured Q when
378 available (DOY 147 to 275) and simulated Q for the remainder of the year (Figure 3a).
379 This gives a total Q of 9.2 km³ yr⁻¹ (251 mm yr⁻¹). For the ungauged section of the
380 basin (27,648 km²) we bias adjust simulated monthly 2002–2010 R in months July,
381 August and September assuming the ratio of simulated to observed at Umiat applies
382 to the lower subbasin. This scaling for the ungauged subbasin produces 4.8 km³ yr⁻¹,
383 and combined with the discharge volume for the Umiat subbasin of 9.2 km³ yr⁻¹ gives
384 14.0 km³ yr⁻¹ for the full basin (Table 2). This estimate compares favorably to the
385 16 km³ yr⁻¹ described by Arnborg et al. (1966) based on measurements in 1962, and
386 is lower than the 19.7 km³ yr⁻¹ (2000–2007) from McClelland et al. (2014). PWB
387 simulated Q (1981–2010) for the Sagavanirktok of 3.0 km³ yr⁻¹ is bracketed by the
388 1.6 km³ yr⁻¹ for 2000–2007 estimated by McClelland et al. (2014) and the 6.5 km³
389 yr⁻¹ for 1971–2001 estimated by Rember and Trefry (2004) using USGS data. Our
390 composite estimate for the Colville (14.0 km³ yr⁻¹), measured Q for the Kuparuk
391 (1.4 km³ yr⁻¹) and modeled Q for the Sagavanirktok (3.0 km³ yr⁻¹) totals 18.4 km³
392 yr⁻¹ for the three rivers combined, which is ~~51.9% of the 57.7%~~ of North Slope do-
393 main total annual Q of ~~28.10–31.9~~ km³ yr⁻¹ (Table 2). ~~Those 3 watersheds occupy~~
394 ~~46.2% of the North Slope study domain.~~

395 4.1.1 ~~Cold season discharge (CSD)~~

396 4.2 Cold season discharge (CSD)

397 Cold season (Nov–Apr) discharge (CSD) from the region simulated over the
398 period 1981–2010 (0.116 km³ season⁻¹) is 0.4% of annual total Q, and between
399 0.2–0.3% for each of the Colville, Kuparuk, and Sagavanirktok rivers. In this region
400 nearly all of the CSD occurs during the first half of winter, namely November and
401 December. CSD for the entire North Slope basin, and both the Colville and Kuparuk
402 rivers, increased significantly (Mann-Kendall test, p < 0.05, Table 2, Figure 6). The
403 CSD increase from the Colville is 215% of the long-term average. For the North
404 Slope basin as a whole CSD increased 134% of the long-term average. Increasing
405 CSD is noted for 9.0% of the North Slope domain, and 28.4% of the Colville basin,
406 primarily in headwater catchments of the foothills of the Brooks Range (Figure 5b).
407 In total the affected terrain covers 88,601 km² or 45% of the North Slope drainage.

408 4.3 Fraction of subsurface runoff

409 We examine variations in modeled surface and subsurface R through the year to
410 better understand how warming is altering the hydrological flows. For the region as

411 a whole the fraction of subsurface runoff to total runoff (hereafter (F_{sub}) increased
412 4.4% ($p < 0.01$), a 31% change relative to the 30 yr average of 14%. Both the
413 Colville and Sagavanirktok rivers show statistically significant ($p < 0.05$) increases
414 in F_{sub} , as do 20 of the 40 remaining basins. Significant increases are noted during
415 several months, most widespread in September (58 of 312 ~~grids or grid cells~~, 18.6% of
416 ~~region domain~~) (Figure 7). Conversely, July shows a decrease in F_{sub} , although over
417 less total area (5.4% ~~of domain~~). For June and September the F_{sub} increases average
418 34.8 and 40.2% respectively for the total change over the period. For July the average
419 is -38.3% , with 17 grids showing ~~an increase and two a decrease a decrease and two~~
420 ~~an increase~~. At the annual time scale the increase in F_{sub} is significant (~~$p < 0.05$~~) for
421 24.7% of the study domain, most notably across the northern foothills of the Brooks
422 Range from the western part of the region (Colville basin) eastward and toward the
423 coast (Figure 8). F_{sub} is consistently 100% of total runoff after October. Areas with
424 increasing F_{sub} are co-located with the areas experiencing increasing CSD.

425 Increasing F_{sub} is noted in areas with a significant increase in active-layer thick-
426 ness (ALT), primarily across parts of the northern foothills of the Brooks Range and
427 the smaller basins near 140°W longitude (Figure 9). Statistically significant increases
428 in ALT have been widespread, noted across two thirds (66.7%) of the region. The
429 simulation shows that one fifth ~~of the region~~ (20.2%) of the region experienced a
430 significant increase in both F_{sub} and ALT ($p < 0.05$, Table 3). A fraction of the
431 foothills region (5.1% of domain) is characterized by a positive trend in F_{sub} only.
432 ~~Statistically significant increases in ALT are widespread (66.7%).~~ The ALT trend
433 average for grid cells with a significant increase in F_{sub} only, a significant increase in
434 ALT only, and a significant increase in both are 0.17 , 0.75 , and 1.00 cm yr^{-1} , respec-
435 tively. ~~The relatively high~~ (Figure 10, Table 3). These relatively large ALT increases
436 in areas of significant F_{sub} increase indicate a connection between ~~increased enhanced~~
437 permafrost thaw and subsurface water flow in those areas (Figure 10, Table 3).

438 4.4 Terrestrial water storage

439 Terrestrial water storage (TWS) over a given time interval is defined by the total
440 amount of water stored in snow, soil liquid water, and soil ice as estimated by the
441 model simulation. Over the 1981–2010 period annual average TWS (all 312 domain
442 grids) exhibits a negative trend of approximately -2 mm yr^{-1} ($p < 0.001$, Figure 11).
443 Declines in annual minimum (-1.7 mm yr^{-1}) and maximum TWS (-2.3 mm yr^{-1})
444 are also significant. Among the component storages there is no significant change
445 in ~~snow storage, an increase in minimum soil water amounts, and a decrease~~ SWE
446 over the 30 year period (Figure S7). Increases in regionally averaged maximum

447 ~~and minimum soil liquid water, and decreases~~ in soil ice (~~Figure S7~~~~amounts, are~~
448 ~~significant ($p < 0.01$, modified Mann-Kendall test)~~). The -2 mm yr^{-1} decrease in
449 TWS reflects a decrease in soil ice ~~storage~~ of -2.5 mm yr^{-1} , a (~~insignificant~~) ~~decrease~~
450 ~~in snow~~ ~~decline in SWE~~ of -0.16 mm yr^{-1} , and an increase in soil water storage of
451 0.61 mm yr^{-1} . ~~In addition to the annual averages, significant increases (decreases)~~
452 ~~in soil water (ice) annual minimum and maximum amounts are also noted.~~

453 4.5 Timing of maximum daily discharge

454 Warming and associated changes in snowmelt have the potential to cause shifts
455 in the timing of peak discharge (Q) during the spring freshet period. Maximum
456 spring discharge is determined from the daily ~~model simulated and~~ routed Q for each
457 of the 42 North Slope ~~river basins~~~~domain rivers~~. In the ~~model~~-simulation only one
458 of the 42 basins exhibits a significant shift to earlier maximum daily Q. None show
459 a significant shift to later maximum Q. ~~While many rivers show simulated peak~~
460 ~~discharge shifting nearly one week earlier over the 30 yr period, high interannual~~
461 ~~variability in annual Q renders the changes insignificant at the 95% level.~~ The
462 average date of maximum daily Q across the 42 basin advanced by approximately
463 4.5 days (Figure S8), though the change is ~~not statistically~~ ~~only marginally~~ significant
464 ($p = 0.1$). Maximum daily Q from the region in recent years occurs near DOY 150
465 (end of May), though this estimate is potentially biased ~~8–10 days early~~ based on
466 the comparison of simulated ~~runoff with measurements~~ ~~and observed runoff~~ for the
467 Kuparuk River (subsection 3.3).

468 5 Summary and Discussion

469 Recent studies have investigated how hydrological cycle intensification and per-
470mafrost thaw may alter terrestrial hydrological fluxes and, in turn, materials ~~exports~~
471 ~~export~~ to coastal zones (~~Walvoord and Striegl, 2007; Frey and McClelland, 2009; Rawlins et al., 2010;~~
472 Changes unfolding across high latitude watersheds have the potential to significantly
473 alter water, carbon, and other constituent fluxes, with implications for nearshore
474 ~~Arctic~~ ~~arctic~~ biogeochemical and ecological processes.

475 ~~Simulated runoff from PWBM v3 shows peak~~ ~~Our synthesis of measured data~~
476 ~~and model simulations reveals that approximately $32 \text{ km}^3 \text{ yr}^{-1}$ of freshwater is~~
477 ~~exported by the region's rivers, with 57.7% of the total originating from the Colville,~~
478 ~~Kuparuk, and Sagavanirktok Rivers. Simulated runoff for the Kuparuk River shows~~
479 ~~maximum daily~~ spring discharge that ~~is systematically 8–10~~ ~~exhibits a systematic~~
480 ~~bias of approximately 8~~ days early relative to gauge data. ~~This bias~~ ~~Timing is well~~

481 estimated for the Colville River. The timing bias for the Kuparuk is unrelated to the
482 specification of river flow velocity in the ~~PWBM~~-routing scheme, and ~~more~~-likely due
483 to a combination of errors in air temperature forcing or modeled snowmelt processes
484 (warm bias) that lead to early snowpack thaw, and/or insufficient surface storages
485 in the ~~mode which would model which serve to~~ delay the transfer of water to stream
486 networks. Simulated R timing may improve by better accounting for these ~~delays~~
487 lags in snowmelt runoff. Future studies should investigate how dynamic surface in-
488 undation data ~~being produced-obtained~~ from microwave and radar remote sensing
489 (Schroeder et al., 2010; Du et al., 2016) can be used to constrain surface water stor-
490 age, its partitioning to runoff and evaporation, and flow direction in areas of low
491 topographic relief. The lag in ~~runoff~~-annual runoff for the Kuparuk River in 1996
492 and 2003 highlight how precipitation and antecedent storage conditions can influence
493 the following year's runoff (Bowling et al., 2003; Stuefer et al., 2017).

494 The quantity and quality of freshwater export is expected to change significantly
495 as the Arctic hydrological cycle intensifies and the system transitions toward in-
496 creasing groundwater water flows (Frey et al., 2003; Frey and McClelland, 2009).
497 In this study evidence of change is evident in cold season discharge from the North
498 Slope region over the 30 year (1981-2010) period examined. There is no significant
499 trend in annual total discharge for the region or its rivers. However, we note that
500 the Kuparuk and nearby Putuligayuk River experienced high annual runoff in 2013,
501 2014, and 2015 (Stuefer et al., 2017), consistent with expectations under an inten-
502 sifying arctic hydrological cycle (Wu et al., 2005; Rawlins et al., 2010). Climate
503 models project a future increase in Arctic precipitation that is generally greatest in
504 autumn and winter and smallest in summer, and greatest over the higher latitudes
505 of Eurasia and North America (ACIA, 2005; Kattsov et al., 2007). Higher win-
506 ter snowfall ~~amounts are possible over across~~ the North Slope ~~, which may, in turn,~~
507 ~~lead to higher would likely lead to increased~~ freshwater discharges. ~~Though relatively~~
508 ~~small in magnitude, the simulation produces an increase~~-The model simulation shows
509 increases in cold season discharge of 134% and 215% of the long-term average for
510 the North Slope ~~and Colville basins~~(domain total) and Colville River, respectively.
511 Basins showing a significant increase in cold season discharge cover 45% of the re-
512 gion. Within the Colville basin the ~~change is being driven by processes in headwater~~
513 ~~subbasins~~-changes are greatest in headwater catchments of the northern foothills
514 and mountains of the Brooks Range (Figure 5b). Landscape conditions in those
515 areas strongly ~~influences~~-influence the quality of water exported during the first half
516 of winter, including the solubility, chemical character, and biodegradability of car-
517 bon, nitrogen and other nutrients (Wickland et al., 2018). ~~Mobilization of water~~
518 ~~through permafrost thaw~~-Effects of permafrost thaw on soil infiltration, flowpath

519 length, and subsurface water movement has been identified ~~as factor~~ in the observed
520 rise in ~~winter (low flow) discharge low flows~~ in parts of the Arctic (St. Jacques
521 and Sauchyn, 2009; Smith et al., 2007; Walvoord and Striegl, 2007). ~~As with the~~
522 ~~results of the present study, The controls permafrost exerts have been implicated~~
523 in the observed increase in ~~winter discharge and decrease in~~ the ratio of maximum
524 to minimum monthly discharge in the continuous permafrost regions of the middle
525 and lower ~~part of the~~ Lena River basin ~~reflect the controls permafrost exerts on~~
526 ~~winter discharge (Gautier et al., 2018)(Gautier et al., 2018), linked with increased~~
527 CSD from 1935–1999 (Yang et al., 2002). More broadly, cold-season low-flow is
528 increasing over most of the pan-arctic (Rennermalm et al., 2010).

529 Our results also show changes in the proportion of groundwater runoff for the
530 region as a whole, and individually the Colville, Sagavanirktok, and 22 of the other
531 ~~42–40~~ river basins. Increases are noted across the foothills and higher elevations of
532 the northern Brooks Range. The growing subsurface flows are contributing to the
533 increasing cold season discharge amounts, with the most significant changes in both
534 quantities found across headwaters of several of the larger basins (Colville and Saga-
535 vanirktok), as well as areas near the coast east of approximately 140°W. Increases
536 in both subsurface runoff and cold season discharge are ~~very~~ likely manifestations
537 of climate warming, as active layer thaw depths are highly responsive to warming
538 air temperatures (Hinkel and Nelson, 2003). Approximately 20% of the region, the
539 Brooks Range foothills and smaller watersheds near 140°W, shows significant in-
540 creases in both the fraction of subsurface runoff and active layer thickness. The
541 active layer increase is greatest in those areas experiencing growing subsurface runoff
542 contributions, suggesting a direct connection between thawing soils and changing
543 subsurface flows.

544 A deepening active layer associated with climate warming will ~~very~~ likely lead to
545 a longer unfrozen period in deeper soils (Yi et al., 2019), enhancing subsurface runoff
546 flow. A deeper active layer delays the soil freeze up and increases the amount of liquid
547 pore water. A larger thawed zone permits additional water storage that supports
548 runoff in late autumn, before soils freeze completely. ~~Diffuse lateral groundwater~~
549 ~~flow at the land-water boundary in coastal regions can exerts a strong influence on~~
550 ~~nearshore geochemistry, relative to surface streamflows, in some areas.~~

551 The changes captured in the modeling are consistent with the notion that per-
552 mafrost thaw enhances hydrogeologic connectivity and increases low flows in per-
553 mafrost regions (Bense et al., 2009, 2012; Bring et al., 2016; Lamontagne-Hallé
554 et al., 2018). Observational and modeling studies suggest that permafrost thaw
555 can lead to increased subsurface runoff and cold season discharge, as increasing
556 thickness of the thawed zone and shallow aquifer provide a conduit for flow to rivers

557 [\(Walvoord and Striegl, 2007; Bense et al., 2009; Walvoord and Kurylyk, 2016; Lamontagne-Hallé et al., 2018\)](#)
558 [Alternatively, these change in continuous permafrost zones can also arise where](#)
559 [permafrost is locally discontinuous, or through flow from unfrozen surface water](#)
560 [bodies.](#)

561 Evidence of permafrost thaw and increasing groundwater flow has been reported
562 in ~~recent~~ studies using measurements from arctic rivers. Recent increases in nitrate
563 concentrations and export from the Kuparuk River are consistent with permafrost
564 degradation and deepening flow paths (McClelland et al., 2007). 'Old' carbon mea-
565 sured in Arctic rivers indicates mobilization of pre-industrial organic matter and
566 subsequent transfer to rivers ~~—~~(Schuur et al., 2009; Mann et al., 2015; Dean et al.,
567 2018). St. Jacques and Sauchyn (2009) concluded that increases in winter baseflow
568 and mean annual streamflow in the NWT were caused predominately by climate
569 warming via permafrost thawing that enhances infiltration and deeper flowpaths and
570 hydrological cycle intensification (Frey and McClelland, 2009; Bring et al., 2016). The
571 magnitude of ~~the groundwater subsurface~~ runoff change in the present ~~simulations~~
572 ~~study~~ should be viewed with caution given the intrinsic resolution of model param-
573 eterizations for soil texture, organic layer thickness, and other landscape properties.
574 Our results, however, do point to a close correspondence between active layer thick-
575 ness and subsurface runoff increases across the foothills of the Brooks Range. ~~This~~
576 ~~result suggests~~ [The enhanced changes there suggest](#) that the relatively thin sur-
577 face organic layer and sandy soils in the foothills areas may be seeing a relative
578 larger impact on soil warming and thaw. ~~Consistent with our results, a study~~
579 ~~using~~ [Our results thus lend additional support to findings in other recent studies](#)
580 [pointing to bigger impacts of warming on permafrost thaw in areas with relatively](#)
581 [low vegetation and low soil organic content \(Yi et al., 2019; Jones et al., 2019\).](#) For
582 [example, Yi et al. \(2019\), using the PWBM in a](#) ~~satellite-based modeling framework~~
583 [modeling framework driven with data from remote sensing observations,](#) found that
584 ALT deepening across much of the Brooks Range has been greater than in the tundra
585 to the north (Yi et al., 2018).

586 Consistent with recent warming and associated ALT increases, our results suggest
587 an overall decline (-2 mm yr^{-2}) in terrestrial water storage across the North Slope
588 drainage basin over the 1981–2010 period. This decrease is driven by losses in soil
589 ice, with an increase in liquid water storage which does not fully offset the ice losses.
590 With continued warming it is likely that the timing of snowmelt will advance, with
591 impacts to the timing of peak (maximum daily) spring discharge. Averaged across all
592 42 basins, the date of daily maximum discharge advanced 4.5 days over the 1981–2010
593 period, though the change is ~~not statistically only marginally~~ significant ($p = 0.1$)
594 at the 95% confidence level. Individual river basins show larger ~~and more significant~~

595 shifts to earlier maximum ~~discharge~~daily discharge. Future changes toward earlier
596 peak discharge can be expected given projections of future warming.

597 Modeling studies of the impacts of climate warming on permafrost thaw and
598 groundwater discharge are key to our understanding of lateral hydrological flows and
599 associated constituent exports. ~~Given uncertainties in solid precipitation amounts~~
600 ~~results~~The underestimate in summer runoff for the Colville River is likely attributable
601 to errors in the meteorological forcings and the model simulation of fluxes including
602 snow sublimation and evapotranspiration. Solid precipitation observations in this
603 region are highly uncertain (Scaff et al., 2015), and this lack of information hinders
604 verification of reanalysis precipitation products and associated studies of changes in
605 seasonal precipitation, which may be playing a role in the hydrological alterations.
606 Results of this study should be corroborated through evaluation of simulations pro-
607 duced with alternate forcings and through parameter sensitivity analysis. The good
608 agreement for the Kuparuk River and the underestimate in simulated discharge
609 for the Umiat subbasin of the Colville point to the need for improved estimates of
610 precipitation across higher elevations of the Brooks Range. A fuller understanding
611 of the extent of water cycle alterations in this region will require new ~~measurements of~~
612 ~~storage and flux terms along with continued development of numerical models~~observations
613 of river discharge, precipitation, snow storage, soil moisture and other key variables
614 needed to parameterize and validate numerical models, including those which capture
615 the important role ground ice plays in runoff generating processes. ~~New discharge~~
616 ~~observations outside of the freshet period, and in un-gaged basins, and associated~~
617 ~~geochemical sampling can be useful to partition surface and groundwater amounts~~Data
618 being gathered within the region's watersheds and coastal environments can provide
619 important information for model parametrization and verification. Measurements of
620 river discharge and dissolved organic carbon at multiple locations along the coast
621 are critical to an improved understanding of land-ocean carbon exports. Regarding
622 linkages with biogeochemical fluxes, water samples from the mouths of major Arctic
623 river show that dissolved organic carbon in those rivers is sourced primarily from
624 fresh vegetation during the two month of spring freshet and from older, soil-, peat-,
625 and wetland-derived DOC during groundwater dominated low flow conditions (Amon
626 et al., 2012). Stable isotope data obtained from river water samples can be used to
627 guide partitioning of surface and groundwater water flows to better understand how
628 soil drainage and soil moisture redistribution will change with future permafrost thaw
629 and ALT deepening (Walvoord and Kurylyk, 2016).

630 High performance computing is ~~shedding~~helping to provide insights into hydro-
631 logical flows and biogeochemical cycling in arctic environments (Lamontagne-Hallé
632 et al., 2018; Neilson et al., 2018). Improvements in numerical model simulations of

633 groundwater flow regimes in permafrost areas have ~~helped to shed insight provided~~
634 insights on the important roles that microtopography and soil properties play in
635 groundwater runoff regimes. Model calibration and validation for simulations at
636 finer spatial scales is dependent on new field measurements of parameters such as
637 water table height, active layer thickness, and soil organic carbon content with depth.
638 Simulations for future conditions in the region should take into account processes di-
639 rectly influenced by permafrost thaw (Bense et al., 2012; Lamontagne-Hallé et al.,
640 2018). To overcome challenges in deriving parameterization from multiple disparate
641 data sets, high-resolution ecosystem maps of the Alaska North Slope can provide a
642 convenient upscaling mechanism to parameterize ground soil properties across the
643 region (Nicolosky et al., 2017). Given its considerable effect on soil thermal and hy-
644 draulic properties, modeling efforts will benefit from improved mapping of soil organic
645 matter. ~~Measurements and modeling of fluvial biogeochemistry can also help shed~~
646 ~~insight on changing watershed characteristics influencing water quantity, quality, and~~
647 ~~associated land-ocean exports.~~

648 6 Acknowledgments

649 We thank the editor and three anonymous for comments which helped to improve
650 the manuscript. We thank Jinyang Du for assistance with the surface fractional
651 open water product and Raymond Bradley, John Kimball, and James McClelland
652 for helpful comments on an earlier version of the manuscript. M.A.R acknowl-
653 edges support from the U.S. National Science Foundation, Office of Polar Programs
654 (NSF-OPP-1656026) and U.S. Department of Energy (DE-SC0019462). ~~The authors~~
655 ~~thank Jinyang Du for assistance with the surface fractional open water product and~~
656 ~~Raymond Bradley, John Kimball, and James McClelland for comments on an earlier~~
657 ~~version of the manuscript.~~ Model outputs and ~~code from this study~~ data are available
658 at:
659 <http://www.geo.umass.edu/climate/data/NSdata.html>

660 7 Author Contributions

661 M.A.R designed the study, executed the model simulations, and performed the
662 analysis. L.C, S.L.S., and D.N. contributed data. M.A.R drafted the initial manuscript
663 and all authors contributed to its development and publication.

664 **Competing interests:** The authors declare that they have no conflict of interest.

665 **References**

- 666 ACIA: *Arctic Climate Impact Assessment*, 1042 pp., Cambridge University Press,
667 New York, 2005. 15
- 668 Amon, R., Rinehart, A., Duan, S., Louchouart, P., Prokushkin, A., Guggenberger,
669 G., Bauch, D., Stedmon, C., Raymond, P., Holmes, R., et al.: Dissolved organic
670 matter sources in large Arctic rivers, *Geochimica et Cosmochimica Acta*, 94, 217–
671 237, 2012. 18
- 672 Arnborg, L., Walker, H. J., and Peippo, J.: Water Discharge in the Colville River,
673 1962, *Geografiska Annaler: Series A, Physical Geography*, 48, 195–210, 1966. 12
- 674 Bense, V., Ferguson, G., and Kooi, H.: Evolution of shallow groundwater flow sys-
675 tems in areas of degrading permafrost, *Geophysical Research Letters*, 36, 2009. 3,
676 16, 17
- 677 Bense, V. F., Kooi, H., Ferguson, G., and Read, T.: Permafrost degradation as a
678 control on hydrogeological regime shifts in a warming climate, *J. Geophys. Res.*,
679 117, doi:10.1029/2011JF002143, 2012. 16, 19
- 680 Bintanja, R. and Selten, F. M.: Future increases in Arctic precipitation
681 linked to local evaporation and sea-ice retreat, *Nature*, 509, 479–482,
682 doi:http://dx.doi.org/10.1038/nature13259 10.1038/nature13259, 2014. 2
- 683 Boisvert, L. N., Webster, M. A., Petty, A. A., Markus, T., Bromwich, D. H.,
684 and Cullather, R. I.: Intercomparison of Precipitation Estimates over the
685 Arctic Ocean and Its Peripheral Seas from Reanalyses, *Journal of Climate*,
686 31, 8441–8462, doi:10.1175/JCLI-D-18-0125.1, URL [https://doi.org/10.1175/
687 JCLI-D-18-0125.1](https://doi.org/10.1175/JCLI-D-18-0125.1), 2018. 5
- 688 Bowling, L. C., Kane, D. L., Gieck, R. E., Hinzman, L. D., and Lettenmaier, D. P.:
689 The role of surface storage in a low-gradient Arctic watershed, *Water Resources*
690 *Research*, 39, 2003. 10, 15
- 691 Bring, A., Fedorova, I., Dibike, Y., Hinzman, L., Mård, J., Mernild, S., Prowse, T.,
692 Semenova, O., Stuefer, S. L., and Woo, M.-K.: Arctic terrestrial hydrology: A syn-
693 thesis of processes, regional effects, and research challenges, *Journal of Geophysical*
694 *Research: Biogeosciences*, 121, 621–649, 2016. 2, 3, 16, 17

- 695 Brodzik, M. J. and Knowles, K.: EASE-Grid: A Versatile Set of Equal-Area Pro-
696 jections and Grids, in M. Goodchild (Ed.) *Discrete Global Grids*. Santa Barbara,
697 CA, USA: National Center for Geographic Information and Analysis., 2002. 4, 1
- 698 Brown, J. and Romanovsky, V. E.: Report from the International Permafrost As-
699 sociation: State of permafrost in the first decade of the 21st century, *Permafrost*
700 *Periglacial Proc.*, 19, 255–260, 2008. 3
- 701 Cai, L., Alexeev, V. A., Arp, C. D., Jones, B. M., Liljedahl, A. K., and Gädeke,
702 A.: The Polar WRF Downscaled Historical and Projected Twenty-First Cen-
703 tury Climate for the Coast and Foothills of Arctic Alaska, *Frontiers in Earth*
704 *Science*, 5, 111, doi:10.3389/feart.2017.00111, URL [https://www.frontiersin.](https://www.frontiersin.org/article/10.3389/feart.2017.00111)
705 [org/article/10.3389/feart.2017.00111](https://www.frontiersin.org/article/10.3389/feart.2017.00111), 2018. 5
- 706 Chadburn, S., Burke, E., Cox, P., Friedlingstein, P., Hugelius, G., and Westermann,
707 S.: An observation-based constraint on permafrost loss as a function of global
708 warming, *Nature Climate Change*, 7, 340, 2017. 3
- 709 Clilverd, H. M., White, D. M., Tidwell, A. C., and Rawlins, M. A.: The Sensitivity of
710 Northern Groundwater Recharge to Climate Change: A Case Study in Northwest
711 Alaska, *Journal of the American Water Resources Association*, pp. 1–13, 2011. 6
- 712 Dean, J., van der Velde, Y., Garnett, M. H., Dinsmore, K. J., Baxter, R., Lessels,
713 J. S., Smith, P., Street, L. E., Subke, J.-A., Tetzlaff, D., et al.: Abundant pre-
714 industrial carbon detected in Canadian Arctic headwaters: implications for the
715 permafrost carbon feedback, *Environmental Research Letters*, 13, 034024, 2018.
716 17
- 717 Dee, D. P., Uppala, S. M., Simmons, A., Berrisford, P., Poli, P., Kobayashi, S.,
718 Andrae, U., Balmaseda, M., Balsamo, G., Bauer, d. P., et al.: The ERA-Interim
719 reanalysis: Configuration and performance of the data assimilation system, *Quar-*
720 *terly Journal of the royal meteorological society*, 137, 553–597, 2011. 5
- 721 Du, J., Kimball, J. S., Jones, L., and Watts, J. D.: Implementation of satellite based
722 fractional water cover indices in the pan-Arctic region using AMSR-E and MODIS,
723 *Remote Sensing of Environment*, 184, 469–481, 2016. 15
- 724 Du, J., Kimball, J. S., Duguay, C., Kim, Y., and Watts, J. D.: Satellite microwave
725 assessment of Northern Hemisphere lake ice phenology from 2002 to 2015, *The*
726 *Cryosphere*, 11, 47, 2017. 6

- 727 Food and Agriculture Organization/UNESCO, 1995: Digital Soil Map of the World
728 and Derived Properties, version 3.5, November, 1995. Original scale 1:5,000000,
729 UNESCO, Paris, France, 1995. 2
- 730 Francis, J. A., Cassano, J. J., Gutowski Jr., W. J., Hinzman, L. D., Holland, M. M.,
731 Steele, M. A., White, D. M., and Vörösmarty, C. J.: An Arctic Hydrologic System
732 in Transition: Feedbacks and Impacts on Terrestrial, Marine, and Human Life, *J.*
733 *Geophys. Res.*, 114, G04019, doi:10.1029/2008JG000902, 2009. 2
- 734 Frey, K. E. and McClelland, J. W.: Impacts of permafrost degradation on arctic river
735 biogeochemistry, *Hydrol. Processes*, 23, 169–182, doi:10.1002/hyp.7196, 2009. 3,
736 14, 15, 17
- 737 Frey, K. E. and Smith, L. C.: Amplified carbon release from vast West Siberian
738 peatlands by 2100, *Geophysical Research Letters*, 32, doi:10.1029/2004GL022025,
739 URL <http://dx.doi.org/10.1029/2004GL022025>, 2005. 3
- 740 Frey, K. E., McClelland, J. W., Holmes, R. M., and Smith, L. C.: Impacts of climate
741 warming and permafrost thaw on the riverine transport of nitrogen and phosphorus
742 to the Kara Sea, *J. Geophys. Res.*, 112, g04S58, DOI:10.1029/2006JG000369,
743 2003. 15
- 744 Gautier, E., Dépret, T., Costard, F., Virmoux, C., Fedorov, A., Grancher, D., Kon-
745 stantinov, P., and Brunstein, D.: Going with the flow: Hydrologic response of
746 middle Lena River (Siberia) to the climate variability and change, *Journal of Hy-*
747 *drology*, 557, 475–488, 2018. 16
- 748 Hamed, K. H. and Rao, A. R.: A modified Mann-Kendall trend test for autocorre-
749 lated data, *Journal of hydrology*, 204, 182–196, 1998. 8
- 750 Hinkel, K. and Nelson, F.: Spatial and temporal patterns of active layer thickness
751 at Circumpolar Active Layer Monitoring (CALM) sites in northern Alaska, 1995–
752 2000, *Journal of Geophysical Research: Atmospheres*, 108, 2003. 16
- 753 Hugelius, G., Strauss, J., Zubrzycki, S., Harden, J. W., Schuur, E., Ping, C.-L.,
754 Schirrmeister, L., Grosse, G., Michaelson, G. J., Koven, C. D., et al.: Estimated
755 stocks of circumpolar permafrost carbon with quantified uncertainty ranges and
756 identified data gaps, *Biogeosciences*, 11, 6573–6593, 2014. 7, 2

- 757 Jones, M. K. W., Pollard, W. H., and Jones, B. M.: Rapid initialization
758 of retrogressive thaw slumps in the Canadian high Arctic and their re-
759 sponse to climate and terrain factors, *Environmental Research Letters*, 14,
760 doi:<https://doi.org/10.1088/1748-9326/ab12fd>, 2019. 17
- 761 Jorgenson, M., Yoshikawa, K., Kanevskiy, M., Shur, Y., Romanovsky, V.,
762 Marchenko, S., Grosse, G., Brown, J., and Jones, B.: Permafrost characteristics
763 of Alaska, in: *Proceedings of the Ninth International Conference on Permafrost*,
764 vol. 3, pp. 121–122, University of Alaska: Fairbanks, 2008. 4
- 765 Kaiser, K., Canedo-Oropeza, M., McMahon, R., and Amon, R. M.: Origins and
766 transformations of dissolved organic matter in large Arctic rivers, *Scientific reports*,
767 7, 13 064, 2017. 3
- 768 Kane, D. and Stuefer, S.: Reflecting on the status of precipitation data collection in
769 Alaska: a case study, *Hydrol Res.*, 46, 478–493, 2015. 5
- 770 Kattsov, V. M., Walsh, J. E., Chapman, W. L., Govorkova, V. A., Pavlova, T. V.,
771 and Zhang, X.: Simulation and Projection of Arctic Freshwater Budget Compo-
772 nents by the IPCC AR4 Global Climate Models, *J. Hydrometeorol.*, 8, 571–589,
773 doi:10.1175/JHM575.1, 2007. 2, 15
- 774 Kistler, R., Kalnay, E., Collins, W., Saha, S., White, G., Woolen, J., Chelliah, M.,
775 Ebisuzaki, W., Kanamitsu, M., Kousky, V., van den Dool, H., Jenne, R., and
776 Fiorino, M.: The NCEP-NCAR 50-year reanalysis: Monthly means CD-ROM and
777 documentation, *Bull. Am. Meteorol. Soc.*, 82, 247–267, 2001. 5
- 778 Lamontagne-Hallé, P., McKenzie, J. M., Kurylyk, B. L., and Zipper, S. C.: Chang-
779 ing groundwater discharge dynamics in permafrost regions, *Environmental Re-*
780 *search Letters*, 13, 084017, URL [http://stacks.iop.org/1748-9326/13/i=8/](http://stacks.iop.org/1748-9326/13/i=8/a=084017)
781 [a=084017](http://stacks.iop.org/1748-9326/13/i=8/a=084017), 2018. 16, 17, 18, 19
- 782 Mann, P. J., Eglinton, T. I., McIntyre, C. P., Zimov, N., Davydova, A., Vonk, J. E.,
783 Holmes, R. M., and Spencer, R. G.: Utilization of ancient permafrost carbon in
784 headwaters of Arctic fluvial networks, *Nature communications*, 6, 2015. 17
- 785 McClelland, J. W., Stieglitz, M., Pan, F., Holmes, R. M., and Peterson, B. J.: Recent
786 changes in nitrate and dissolved organic carbon export from the upper Kuparuk
787 River, *J. Geophys. Res.*, 112, g04S60, doi:10.1029/2006JG000371, 2007. 17

- 788 McClelland, J. W., Townsend-Small, A., Holmes, R. M., Pan, F., Stieglitz, M.,
789 Khosh, M., and Peterson, B. J.: River export of nutrients and organic matter
790 from the North Slope of Alaska to the Beaufort Sea, *Water Resources Research*,
791 50, 1823–1839, 2014. 11, 12
- 792 Miller, J. R., Russell, G. L., and Caliri, G.: Continental-scale river flow in climate
793 models, *Journal of Climate*, 7, 914–928, 1994. 8
- 794 Neilson, B. T., Cardenas, M. B., O’Connor, M. T., Rasmussen, M. T., King, T. V.,
795 and Kling, G. W.: Groundwater Flow and Exchange Across the Land Surface
796 Explain Carbon Export Patterns in Continuous Permafrost Watersheds, *Geo-*
797 *physical Research Letters*, 0, doi:10.1029/2018GL078140, URL [https://agupubs.](https://agupubs.onlinelibrary.wiley.com/doi/abs/10.1029/2018GL078140)
798 [onlinelibrary.wiley.com/doi/abs/10.1029/2018GL078140](https://agupubs.onlinelibrary.wiley.com/doi/abs/10.1029/2018GL078140), in press, 2018. 3,
799 18
- 800 Nicolsky, D. J., Romanovsky, V., Panda, S., Marchenko, S., and Muskett, R.: Appli-
801 cability of the ecosystem type approach to model permafrost dynamics across the
802 Alaska North Slope, *Journal of Geophysical Research: Earth Surface*, 122, 50–75,
803 2017. 5, 6, 7, 19, 3, 4
- 804 Peterson, B. J., Holmes, R. M., McClelland, J. W., Vörös-
805 marty, C. J., Lammers, R. B., Shiklomanov, A. I., Shiklomanov,
806 I. A., and Rahmstorf, S.: Increasing river discharge to the Arc-
807 tic Ocean, *Science*, 298, 2171–2173, doi:10.1126/science.1077445,
808 <http://www.sciencemag.org/content/298/5601/2171.short>, 2002. 2
- 809 Peterson, B. J., McClelland, J., Curry, R., Holmes, R. M., Walsh,
810 J. E., and Aagaard, K.: Trajectory shifts in the Arctic and sub-
811 Arctic freshwater cycle, *Science*, 313, 1061–1066, doi:10.1126/science.1122593,
812 <http://www.sciencemag.org/content/313/5790/1061.short>, 2006. 2
- 813 Rawlins, M., Nicolsky, D., McDonald, K., and Romanovsky, V.: Simulating soil
814 freeze/thaw dynamics with an improved pan-Arctic water balance model, *Journal*
815 *of Advances in Modeling Earth Systems*, 5, 659–675, doi:10.1002/jame.20045, URL
816 <http://dx.doi.org/10.1002/jame.20045>, 2013. 5, 6, 7
- 817 Rawlins, M. A., Lammers, R. B., Frohling, S., Fekete, B. M., and Vörösmarty,
818 C. J.: Simulating Pan-Arctic Runoff with a Macro-Scale Terrestrial Water Bal-
819 ance Model, *Hydrol. Processes*, 17, 2521–2539, 2003. 5, 6

- 820 Rawlins, M. A., Fahnestock, M., Frohling, S., and Vörösmarty, C. J.: On the Eval-
821 uation of Snow Water Equivalent Estimates over the Terrestrial Arctic Drainage
822 Basin, *Hydrol. Processes*, 21, 1616–1623, doi: 10.1002/hyp.6724, 2007. 6
- 823 Rawlins, M. A., Serreze, M. C., Schroeder, R., Zhang, X., and McDonald, K. C.:
824 Diagnosis of the Record Discharge of Arctic-Draining Eurasian Rivers in 2007,
825 *Environ. Res. Lett.*, 4, 045011, doi: 10.1088/1748-9326/4/4/045011, 2009. 6
- 826 Rawlins, M. A., Steele, M., Holland, M. M., Adam, J. C., Cherry,
827 J. E., Francis, J. A., Groisman, P. Y., Hinzman, L. D., Hunting-
828 ton, T. G., Kane, D. L., and Coauthors: Analysis of the Arctic
829 System for Freshwater Cycle Intensification: Observations and Expecta-
830 tions, *J. Clim.*, 23, 5715–5737, doi:http://dx.doi.org/10.1175/2010JCLI3421.1,
831 http://journals.ametsoc.org/doi/abs/10.1175/2010JCLI3421.1, 2010. 2, 14, 15
- 832 Rember, R. D. and Trefry, J. H.: Increased concentrations of dissolved trace metals
833 and organic carbon during snowmelt in rivers of the Alaskan Arctic, *Geochimica
834 et Cosmochimica Acta*, 68, 477–489, 2004. 12
- 835 Rennermalm, A. K., Wood, E. F., and Troy, T. J.: Observed changes in pan-arctic
836 cold-season minimum monthly river discharge, *Climate dynamics*, 35, 923–939,
837 2010. 16
- 838 Rienecker, M., Suarez, M., Gelaro, R., Todling, R., Bacmeister, J., Liu, E.,
839 Bosilovich, M., Schubert, S., Takacs, L., Kim, G., et al.: MERRA-NASA’s
840 Modern-Era Retrospective Analysis for Research and Applications, *Bulletin of
841 the American Meteorological Society*, 2011. 5
- 842 Romanovsky, V. E., Smith, S. L., and Christiansen, H. H.: Permafrost thermal state
843 in the polar Northern Hemisphere during the international polar year 2007–2009:
844 a synthesis, *Permafrost Periglacial Proc.*, 21, 106–116, doi:10.1002/ppp.689, URL
845 http://dx.doi.org/10.1002/ppp.689, 2010. 3
- 846 Scaff, L., Yang, D., Li, Y., and Mekis, E.: Inconsistency in precipitation measure-
847 ments across the Alaska–Yukon border, *The Cryosphere*, 9, 2417–2428, 2015. 18
- 848 Schroeder, R., McDonald, K. C., Zimmerman, R., Podest, E., and Rawlins, M.:
849 North Eurasian Inundation Mapping with Passive and Active Microwave Remote
850 Sensing, *Environ. Res. Lett.*, 5, 015003, doi:10.1088/1748-9326, 2010. 6, 15

- 851 Schuur, E., Vogel, J. G., Crummer, K. G., Lee, H., Sickman, J. O., and Osterkamp,
852 T. E.: The effect of permafrost thaw on old carbon release and net carbon exchange
853 from tundra, *Nature*, 459, 556–559, 2009. 17
- 854 Serreze, M. C., Barrett, A. P., Slater, A. G., Woodgate, R. A., Aagaard, K., Lam-
855 mers, R. B., Steele, M., Moritz, R., Meredith, M., and Lee, C. M.: The large-scale
856 freshwater cycle of the Arctic, *J. Geophys. Res.*, 111, doi:10.1029/2005JC003424,
857 <http://onlinelibrary.wiley.com/doi/10.1029/2005JC003424/full>, 2006. 2
- 858 Serreze, M. C., Barrett, A. P., and Stroeve, J.: Recent changes in tropospheric
859 water vapor over the Arctic as assessed from radiosondes and atmospheric
860 reanalyses, *Journal of Geophysical Research: Atmospheres* (1984–2012), 117,
861 doi:10.1029/2011JD017421, 2012. 3
- 862 Shiklomanov, I. A., Shiklomanov, A. I., Lammers, R. B., Peterson, B. J., and Vörös-
863 marty, C. J.: The dynamics of river water inflow to the Arctic Ocean, pp. 281–296,
864 Kluwer Academic Press, Dordrecht, in *The Freshwater Budget of the Arctic Ocean*,
865 edited by E.I Lewis, et al., 2000. 2
- 866 Smith, L. C., Pavelsky, T. M., MacDonald, G. M., Shiklomanov, A. I., and Lammers,
867 R. B.: Rising minimum daily flows in northern Eurasian rivers: A growing influence
868 of groundwater in the high-latitude hydrologic cycle, *J. Geophys. Res.*, 112, g04S47,
869 doi:10.1029/2006JG000327, 2007. 16
- 870 Smith, S., Romanovsky, V., Lewkowicz, A., Burn, C., Allard, M., Clow, G.,
871 Yoshikawa, K., and Throop, J.: Thermal state of permafrost in North Amer-
872 ica: a contribution to the international polar year, *Permafrost Periglacial Proc.*,
873 21, 117–135, doi:10.1002/ppp.690, URL <http://dx.doi.org/10.1002/ppp.690>,
874 2010. 3
- 875 Spencer, R. G., Mann, P. J., Dittmar, T., Eglinton, T. I., McIntyre, C., Holmes,
876 R. M., Zimov, N., and Stubbins, A.: Detecting the signature of permafrost thaw
877 in Arctic rivers, *Geophysical Research Letters*, 42, 2830–2835, 2015. 14
- 878 St. Jacques, J. M. and Sauchyn, D. J.: Increasing winter baseflow and mean annual
879 streamflow from possible permafrost thawing in the Northwest Territories, Canada,
880 *Geophys. Res. Lett.*, 36, L01401, doi:10.1029/2008GL035822, 2009. 3, 16, 17
- 881 Striegl, R. G., Aiken, G. R., Dornblaser, M. M., Raymond, P. A., and Wick-
882 land, K. P.: A decrease in discharge-normalized DOC export by the Yukon
883 River during summer through autumn, *Geophysical Research Letters*, 32,

884 doi:10.1029/2005GL024413, URL <http://dx.doi.org/10.1029/2005GL024413>,
885 2005. 3

886 Stuefer, S., Kane, D. L., and Liston, G. E.: In situ snow water equivalent observations
887 in the US Arctic, *Hydrology Research*, 44, 21–34, 2013. 4, 5

888 Stuefer, S. L., Arp, C. D., Kane, D. L., and Liljedahl, A. K.: Recent Extreme
889 Runoff Observations From Coastal Arctic Watersheds in Alaska, *Water Resources*
890 *Research*, 53, 9145–9163, doi:10.1002/2017WR020567, URL [https://agupubs.
891 onlinelibrary.wiley.com/doi/abs/10.1002/2017WR020567](https://agupubs.onlinelibrary.wiley.com/doi/abs/10.1002/2017WR020567), 2017. 10, 11, 15

892 Vonk, J. E., Tank, S. E., Mann, P. J., Spencer, R. G., Treat, C. C., Striegl, R.,
893 Abbott, B. W., and Wickland, K. P.: Biodegradability of dissolved organic carbon
894 in permafrost soils and aquatic systems: a meta-analysis, *Biogeosciences*, 12, 6915–
895 6930, 2015. 14

896 Vörösmarty, C. J., Fekete, B. M., Maybeck, M., and Lammers, R. B.: Gloabl System
897 of Rivers: Its Role in Organizing Continental Land Mass and Defining Land-to-
898 Ocean Linkages, *Global Biogeochem. Cycles*, 14, 599–621, 2000. 7

899 Walvoord, M. A. and Kurylyk, B. L.: Hydrologic impacts of thawing permafrost—A
900 review, *Vadose Zone Journal*, 15, 2016. 3, 17, 18

901 Walvoord, M. A. and Striegl, R. G.: Increased groundwater to stream discharge from
902 permafrost thawing in the Yukon River basin: Potential impacts on lateral export
903 of carbon and nitrogen, *Geophysical Research Letters*, 34, 2007. 3, 14, 16, 17

904 Wickland, K. P., Waldrop, M. P., Aiken, G. R., Koch, J. C., Jorgenson, M. T., and
905 Striegl, R. G.: Dissolved organic carbon and nitrogen release from boreal Holocene
906 permafrost and seasonally frozen soils of Alaska, *Environmental Research Letters*,
907 13, 065 011, URL <http://stacks.iop.org/1748-9326/13/i=6/a=065011>, 2018.
908 3, 15

909 Willmott, C. J. and Matsuura, K.: Advantages of the mean absolute error (MAE)
910 over the root mean square error (RMSE) in assessing average model performance,
911 *Climate research*, 30, 79, 2005. 8

912 Willmott, C. J., Robeson, S. M., Matsuura, K., and Ficklin, D. L.: Assessment of
913 three dimensionless measures of model performance, *Environmental Modelling &*
914 *Software*, 73, 167–174, 2015. 8

- 915 Wrona, F. J., Johansson, M., Culp, J. M., Jenkins, A., Mård, J., Myers-Smith,
916 I. H., Prowse, T. D., Vincent, W. F., and Wookey, P. A.: Transitions in Arctic
917 ecosystems: Ecological implications of a changing hydrological regime, *Journal of*
918 *Geophysical Research: Biogeosciences*, 121, 650–674, 2016. 3
- 919 Wu, P., Wood, R., and Stott, P.: Human influence on increasing Arctic river dis-
920 charges, *Geophys. Res. Lett.*, 32, L02703, doi:10.1029/2004GL021570, 2005. 3,
921 15
- 922 Yang, D., Goodison, B. E., Ishida, S., and Benson, C. S.: Adjustment of Daily
923 Precipitation Data at 10 Stations in Alaska: Application of World Meteorological
924 Organization Intercomparison Results, *Water Resour. Res.*, 34, 241–256, 1998. 5
- 925 Yang, D., Kane, D. L., Hinzman, L. D., Zhang, X., Zhang, T., and Ye, H.: Siberian
926 Lena River hydrologic regime and recent change, *J. Geophys. Res.*, 107, 4694,
927 doi:10.1029/2002JD002542, 2002. 16
- 928 Yang, D., Kane, D., Zhang, Z., Legates, D., and Goodison, B.: Bias corrections of
929 long-term (1973–2004) daily precipitation data over the northern regions, *Geophys.*
930 *Res. Lett.*, 32, L19501, doi:10.1029/2005GL024057, 2005. 5
- 931 Yi, Y., Kimball, J. S., Jones, L. A., Reichle, R. H., Nemani, R., and Margolis, H. A.:
932 Recent climate and fire disturbance impacts on boreal and arctic ecosystem pro-
933 ductivity estimated using a satellite-based terrestrial carbon flux model, *Journal*
934 *of Geophysical Research: Biogeosciences*, pp. 1–17, 2013. 6
- 935 Yi, Y., Kimball, J. S., Rawlins, M. A., Moghaddam, M., and Euskirchen, E. S.: The
936 role of snow cover affecting boreal-arctic soil freeze/thaw and carbon dynamics,
937 *Biogeosciences*, 12, 5811–5829, 2015. 6
- 938 Yi, Y., Kimball, J. S., Chen, R. H., Moghaddam, M., Reichle, R. H., Mishra, U.,
939 Zona, D., and Oechel, W. C.: Characterizing permafrost active layer dynamics
940 and sensitivity to landscape spatial heterogeneity in Alaska, *The Cryosphere*, 12,
941 145–161, doi:10.5194/tc-12-145-2018, URL [https://www.the-cryosphere.net/](https://www.the-cryosphere.net/12/145/2018/)
942 [12/145/2018/](https://www.the-cryosphere.net/12/145/2018/), 2018. 6, 17
- 943 Yi, Y., Kimball, J. S., Chen, R. H., Moghaddam, M., and Miller, C. E.: Sensitivity of
944 active-layer freezing process to snow cover in Arctic Alaska, *The Cryosphere*, 13,
945 197–218, doi:10.5194/tc-13-197-2019, URL [https://www.the-cryosphere.net/](https://www.the-cryosphere.net/13/197/2019/)
946 [13/197/2019/](https://www.the-cryosphere.net/13/197/2019/), 2019. 6, 16, 17

- 947 Yue, S., Pilon, P., and Cavadias, G.: Power of the Mann–Kendall and Spearman’s rho
948 tests for detecting monotonic trends in hydrological series, *Journal of hydrology*,
949 259, 254–271, 2002. 8
- 950 Zhang, X., He, J., Zhang, J., Polyakov, I., Gerdes, R., Inoue, J., and Wu, P.: En-
951 hanced poleward moisture transport and amplified northern high-latitude wetting
952 trend, *Nature Climate Change*, 3, 47–51, doi:doi:10.1038/nclimate1631, 2013. 2

Table 1: Distribution statistics (cm) for spatial fields of active layer thickness (ALT) from the GIPL and PWBM simulation with MERRA* forcing shown in Figure S3. Also shown are statistics for a simulation using original (non-adjusted) MERRA precipitation (P) data.

Active Layer Thick Distribution Statistics (cm)					
Data	5 th	25 th	mean	75 th	95 th
GIPL	37.3	49.9	55.2	61.4	69.4
PWBM (MERRA)	30.5	40.3	50.4	58.6	75.2
PWBM (MERRA*)	32.0	43.7	53.5	61.3	79.0

Table 2: ~~Basin~~ River basin area, annual discharge (Q), and cold season discharge (CSD) for ~~several North Slope~~ the Colville, Kuparuk, and Sagavanirktok rivers and the full North Slope domain. ~~Basins~~ River basins with a significant increase in CSD are indicated with a superscript *. Basin areas are based on their specification in the simulated topological river network.

River Basin and Domain-Wide Discharge			
Basin	Area (km ²)	Annual Q (km ³ yr ⁻¹)	CSD (km ³ season ⁻¹)
Colville	64 095	10.21 <u>14.0</u>	0.023*
Kuparuk	10 054	1.35 <u>1.4</u>	0.004*
Sagavanirktok	16 338	3.01 <u>3.0</u>	0.006
3 River Total	90 487	14.57 <u>18.4</u>	0.032
North Slope	196 061	28.10 <u>31.9</u>	0.116*

Table 3: Number of grid cells, associated area fraction of domain, and average ALT and F_{sub} for each category shown. ~~Domain~~ Study domain consists of 312 grid cells spanning an area of 196,060.8-060 km² (Figure 1).

Number of grids, area, and ALT and F_{sub} averages for each subregion.				
	N	area (%)	F_{sub} (%³ yr⁻¹)	ALT (cm yr⁻¹)
F_{sub} increase only	16	5.1	0.43	0.17
ALT increase only	211	67.6	0.05	0.75
both	63	20.2	0.35	1.00
neither	22	7.1	0.22	0.22

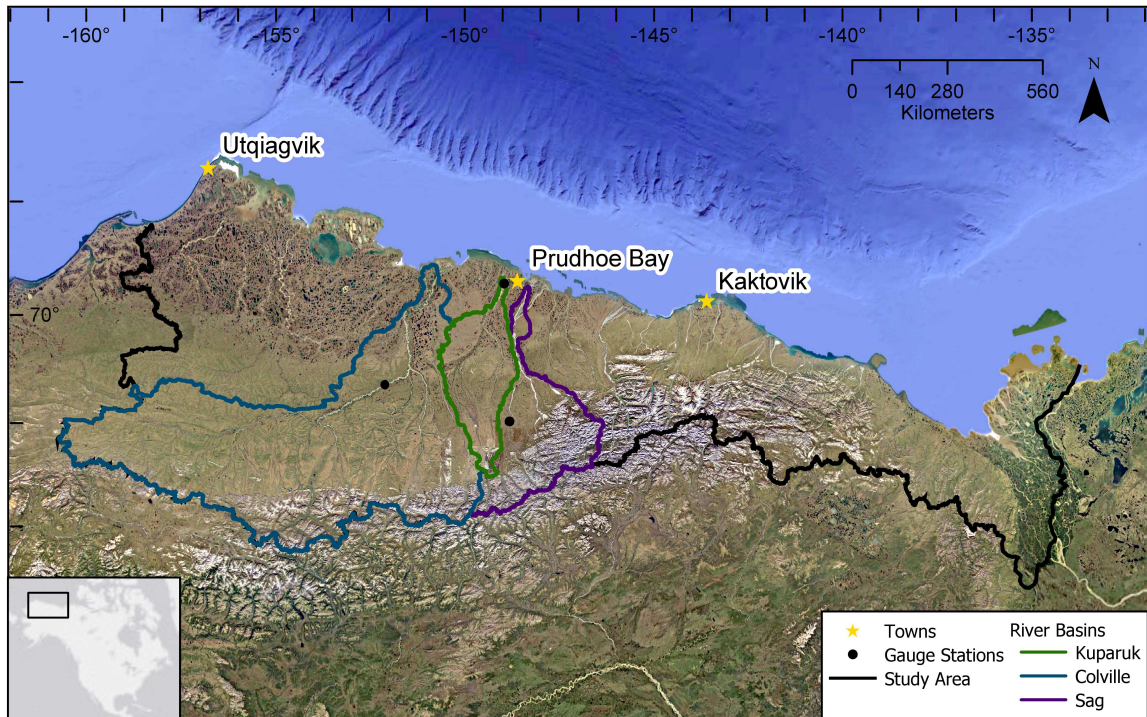


Figure 1: Study domain of North Slope of Alaska. Black line delineates the full North Slope drainage basin. This domain includes all land (196,060 km²) which drains to the Beaufort Sea coast. Blue, green, and purple lines mark boundaries for the drainage basins of the Colville, Kuparuk, and Sagavanirktok rivers, respectively. The three dots mark locations where USGS discharge measurements are obtained for each river at, respectively, Umiat, Deadhorse, and Pump Station #3. The 42 individual basins defined by the simulated topological network (STN) are listed in Table S1. Locations shown for population centers Utqiagvik, Prudhoe Bay, and Kaktovik.

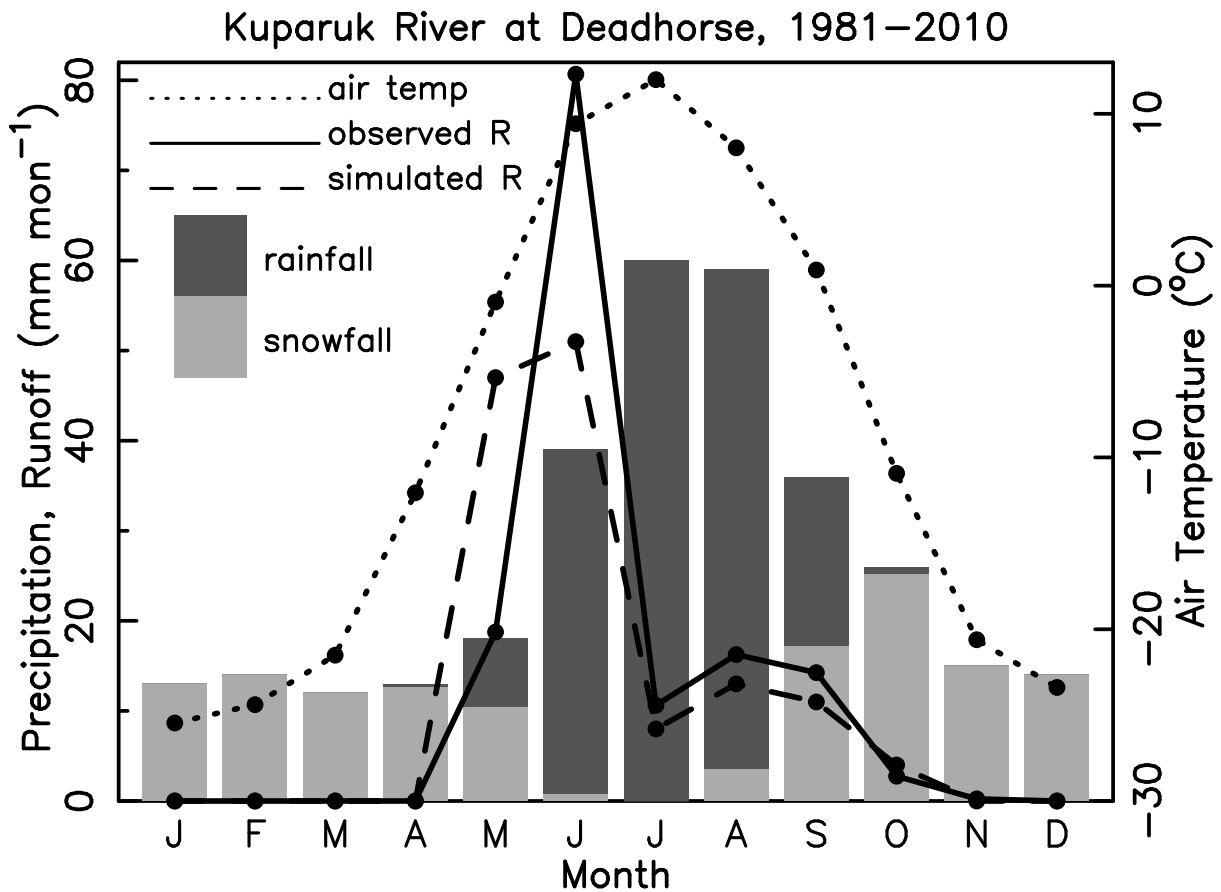


Figure 2: ~~Monthly climatological precipitation (P) and simulated~~ Simulated and observed runoff (R, mm month⁻¹) for the Kuparuk River basin 1981–2010. Simulated R expressed in unit depth was calculated from the routed river discharge (Q) volume Kuparuk. ~~Forcing~~ Observed R was drawn from the USGS database (section 2.1). The PWBM simulation was forced with meteorological data from the MERRA reanalysis, with precipitation adjustment (MERRA*) as described in section 2.2. Monthly air temperature is the average over the Kuparuk basin from the MERRA data used in the model simulation. Monthly climatological precipitation (P) shown in totals (mm month⁻¹) for rainfall and snowfall.

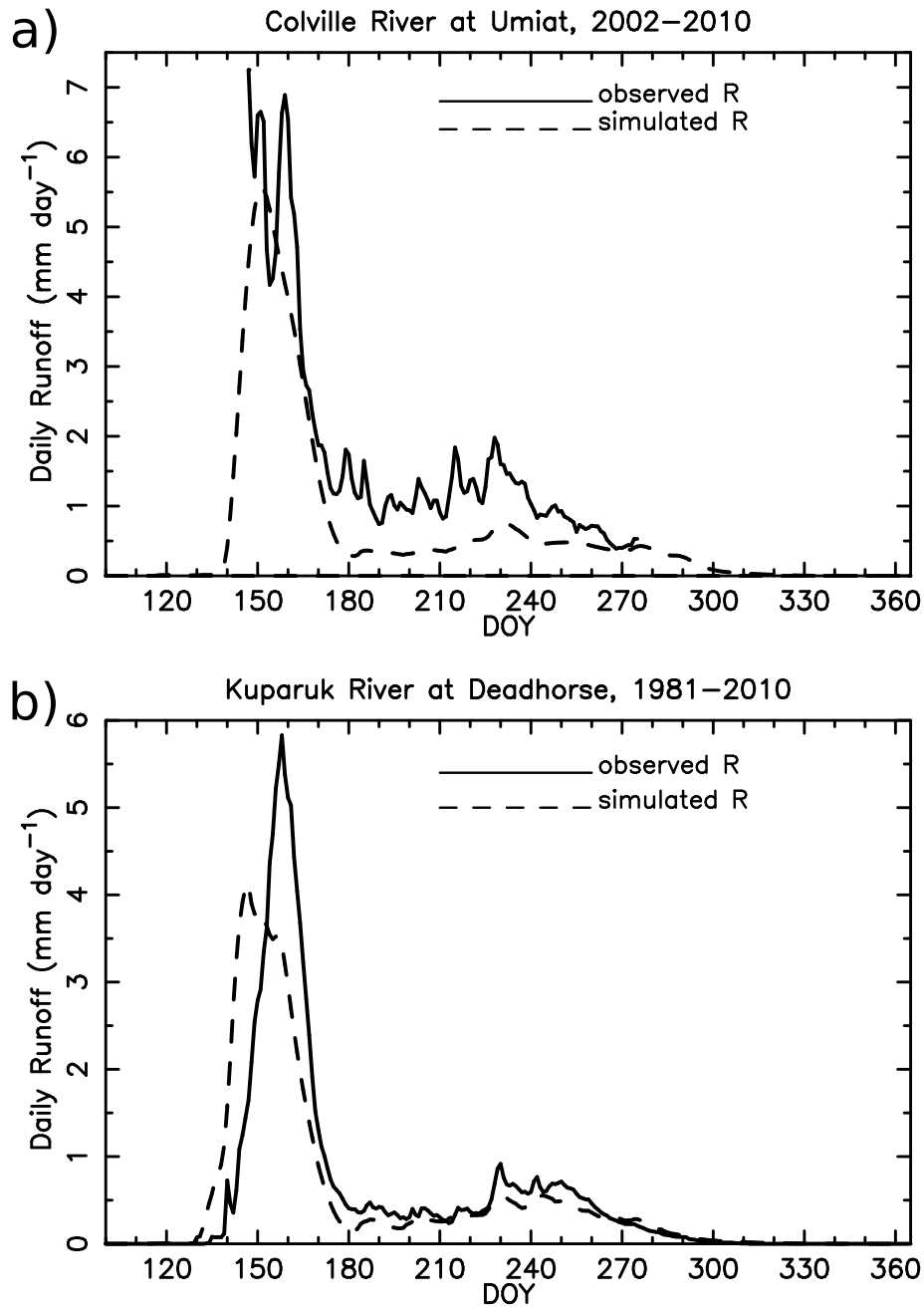


Figure 3: ~~Annual total P from MERRA (adjusted) and simulated~~ Simulated and observed ~~R runoff (R, mm yrday⁻¹) over for the~~ (a) Colville River at Umiat, AK and (b) Kuparuk basin River at Deadhorse AK. Discharge data for the simulation period 1981–2010 Colville River published by the USGS are generally available each year from the end of May until early October. Runoff calculated as unit depth as in Figure 2.

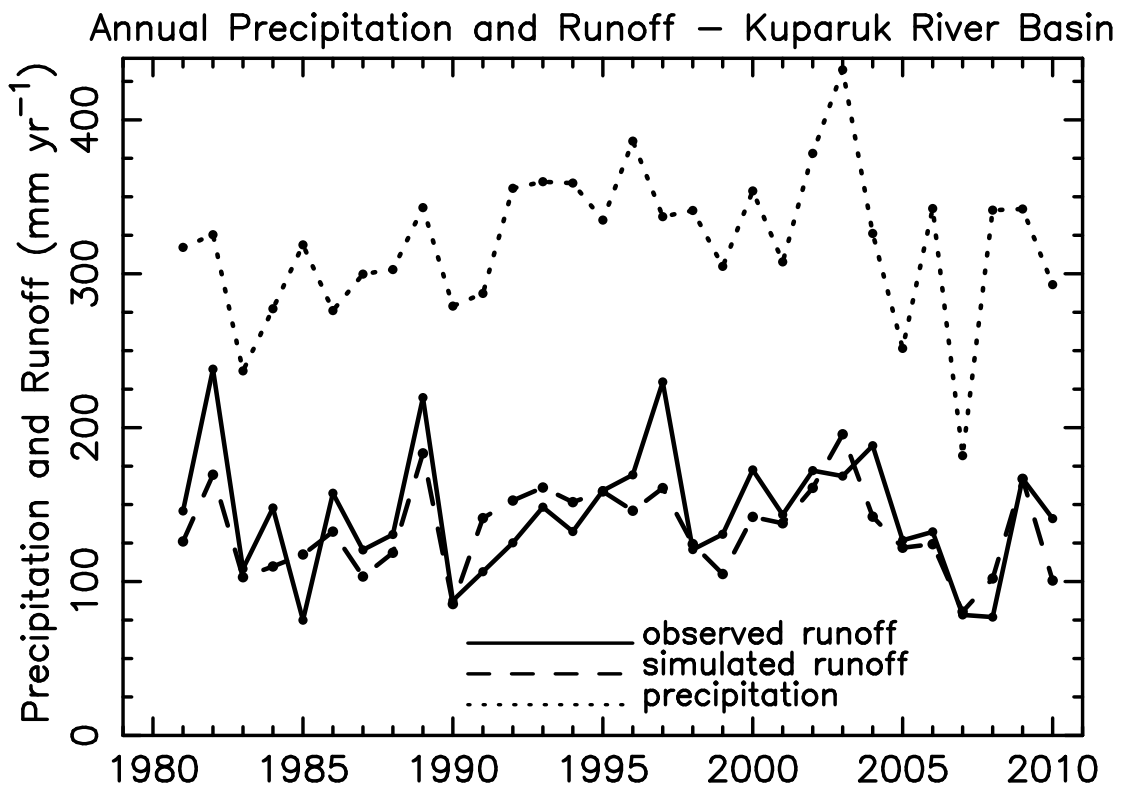


Figure 4: [Annual total P from the adjusted MERRA \(MERRA*, section 2.2\) and simulated and observed R \(mm yr⁻¹\) for the Kuparuk River basin for the simulation period 1981–2010.](#)

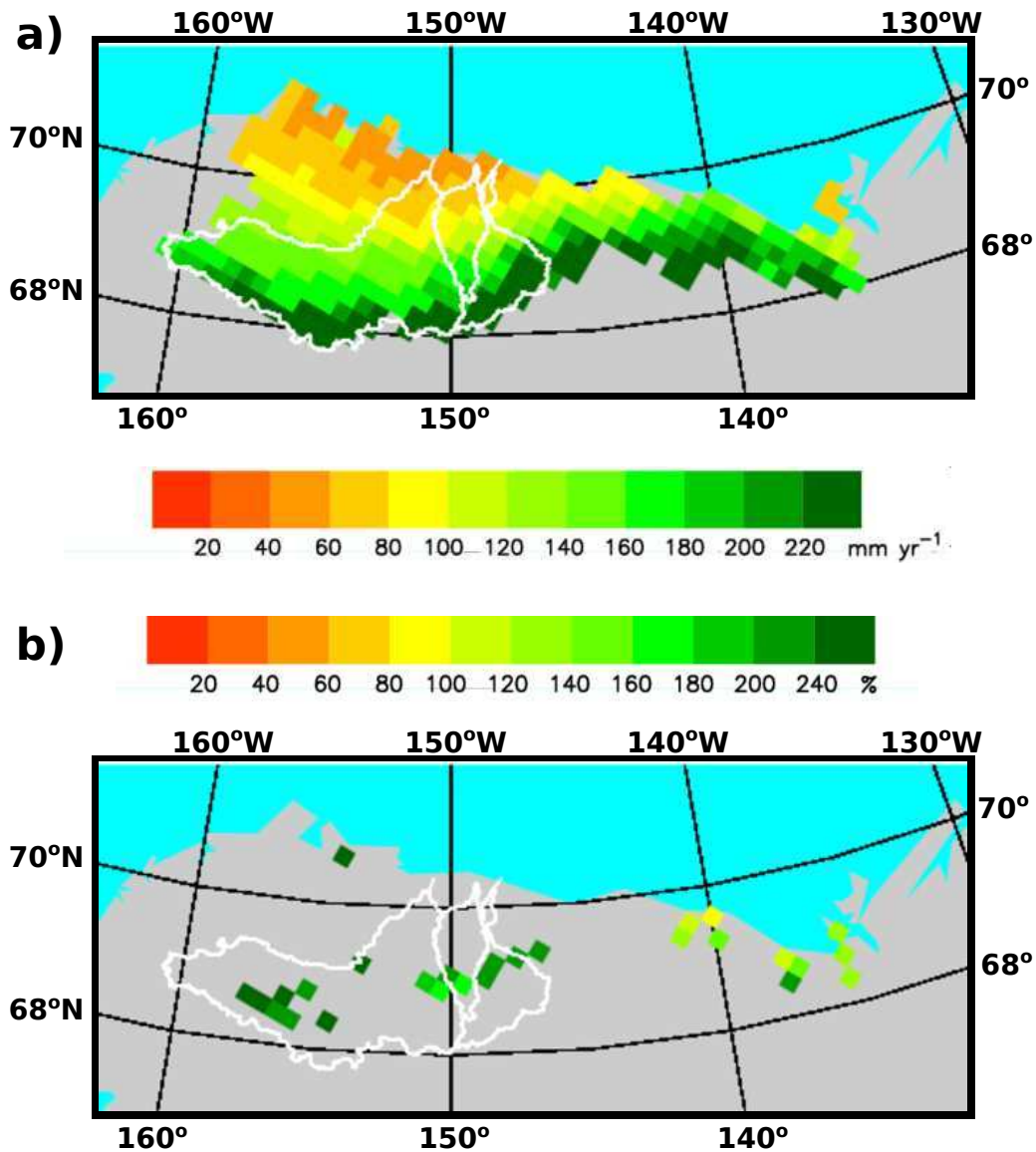


Figure 5: a) Annual total R 1981–2010 (mm yr^{-1}) from the model simulation and b) grid cells with a statistically significant ($p < 0.05$) change in [simulated](#) cold season (Nov–Apr) Q over the period 1981–2010. The change is shaded as a percentage of the 30 yr average for cold season R for that grid. White outlines are basin boundaries for the (west to east) Colville, Kuparuk, and Sagavanirktok rivers.

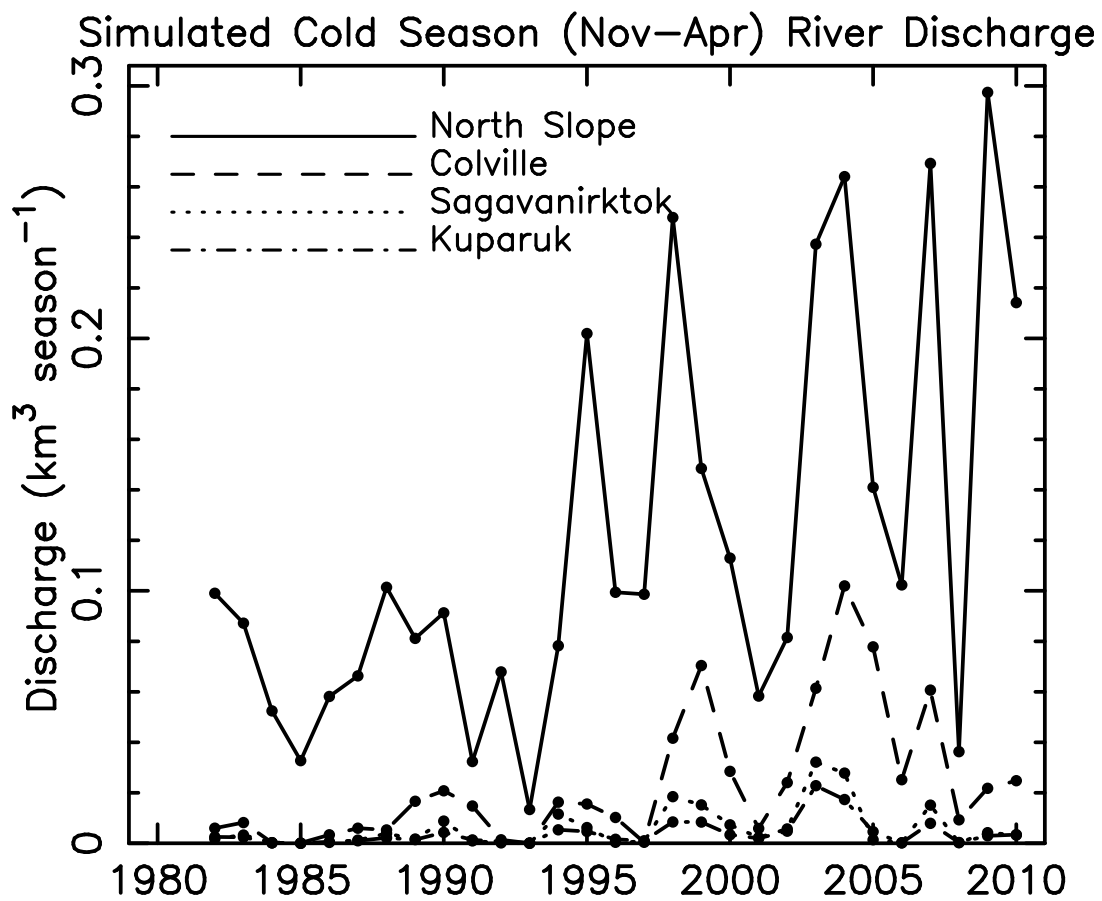


Figure 6: ~~Cold~~ Simulated cold season Q (km³ season⁻¹) for the full North Slope region and for separately the Colville, Sagavanirktok, and Kuparuk Rivers rivers.

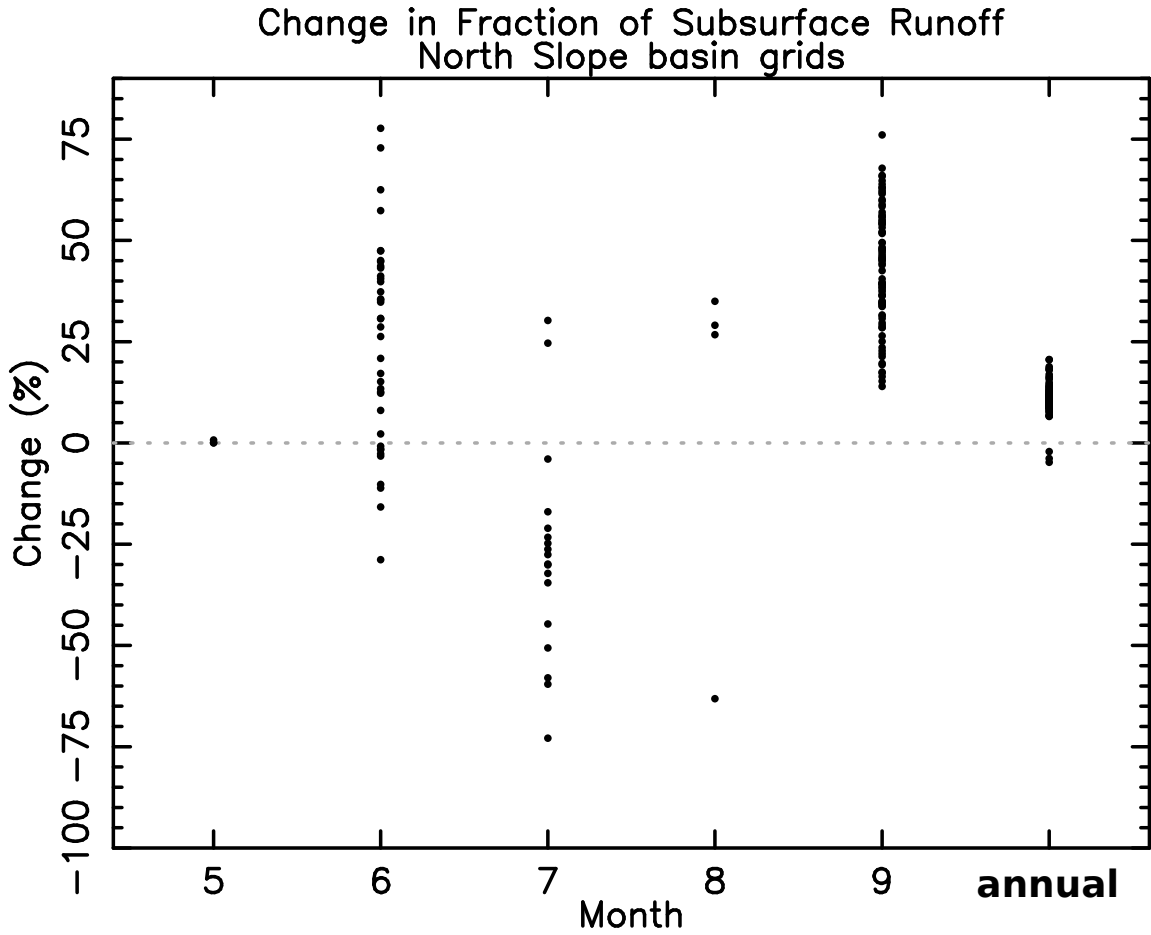


Figure 7: a) ~~Change-Grid cell change~~ in fraction of subsurface R (F_{sub}) for warm season months May–September and for annual total F_{sub} and R. F_{sub} changes are not defined for other months due to F_{sub} consistently at 100%, or the grid cell having no runoff for that month in more than 50% (15 of 30) of the data years. Change is expressed with respect to the long-term average. Dots represent ~~grids-grid cells~~ that show a significant change at $p < 0.05$. Average for grids with a significant change at the annual scale is +11.0%

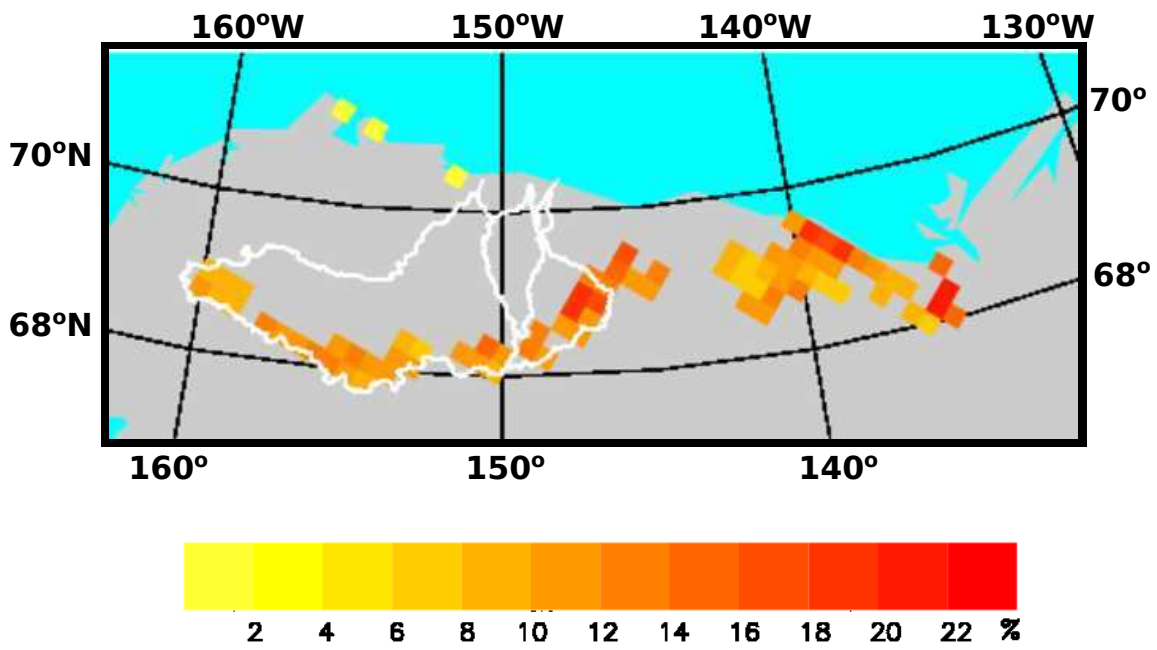


Figure 8: Change in **fraction of subsurface R** (F_{sub} , %) over the period 1981–2010. Mapped grids show a significant change at $p < 0.05$ based on a two-sided t -test.

Regions With Significant Increase in F_{sub} and ALT

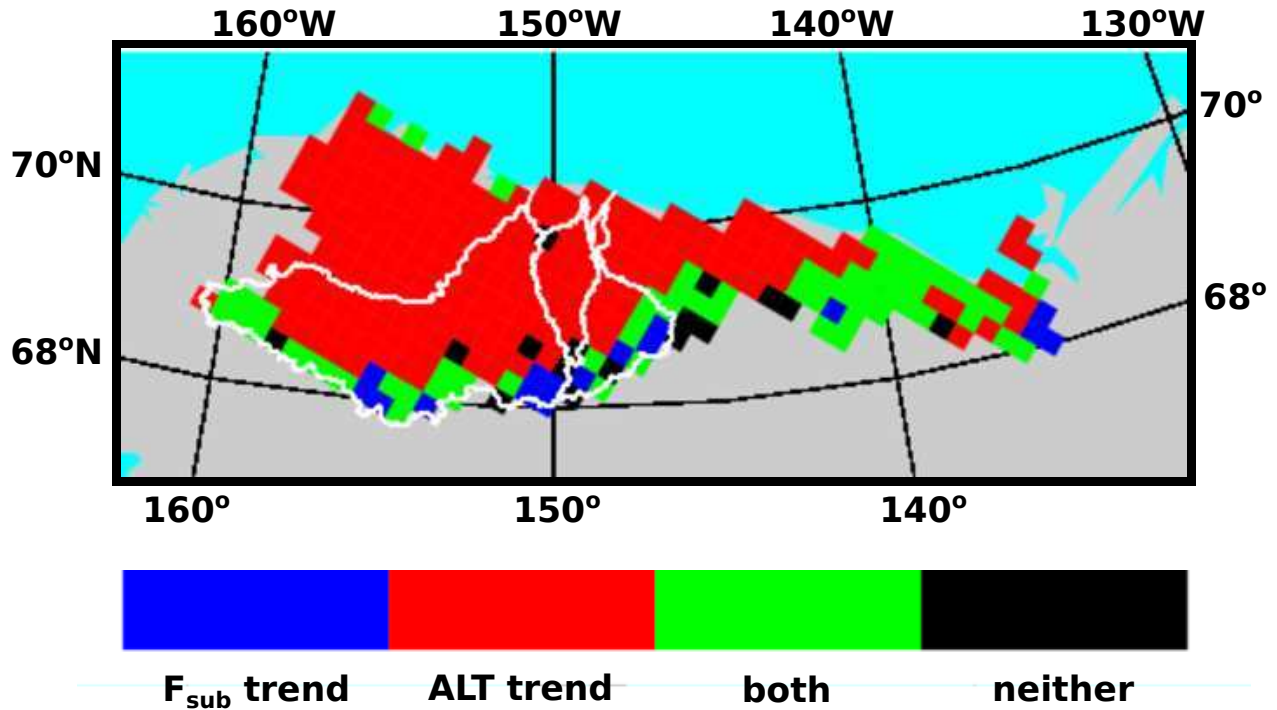


Figure 9: Spatial extent of regions showing a significant increase in annual F_{sub} only (blue), a significant increase in active layer thickness (ALT) only (red), significant increases in both (green), and neither (black). The number of [grid cells](#), area fraction [impacted](#), and average F_{sub} and ALT increase for each category [are](#) shown in Table 3.

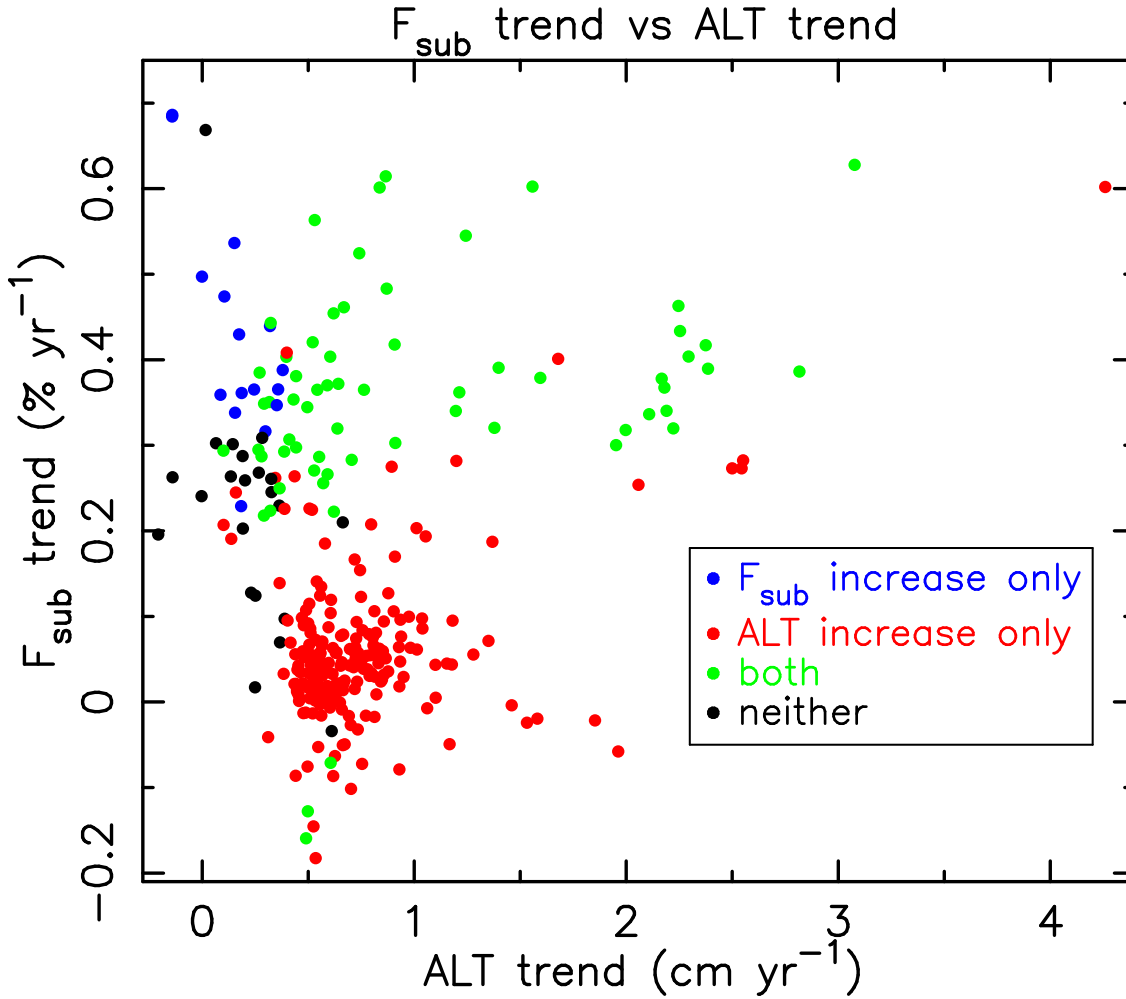


Figure 10: Increase in annual F_{sub} ($\% \text{ yr}^{-1}$) vs increase in seasonal maximum ALT (cm yr^{-1}) for all 312 domain grid cells. ~~The number of grids, areal percent, and average F_{sub} and ALT increase for each category shown~~ Relevant statistics are listed in Table 3.

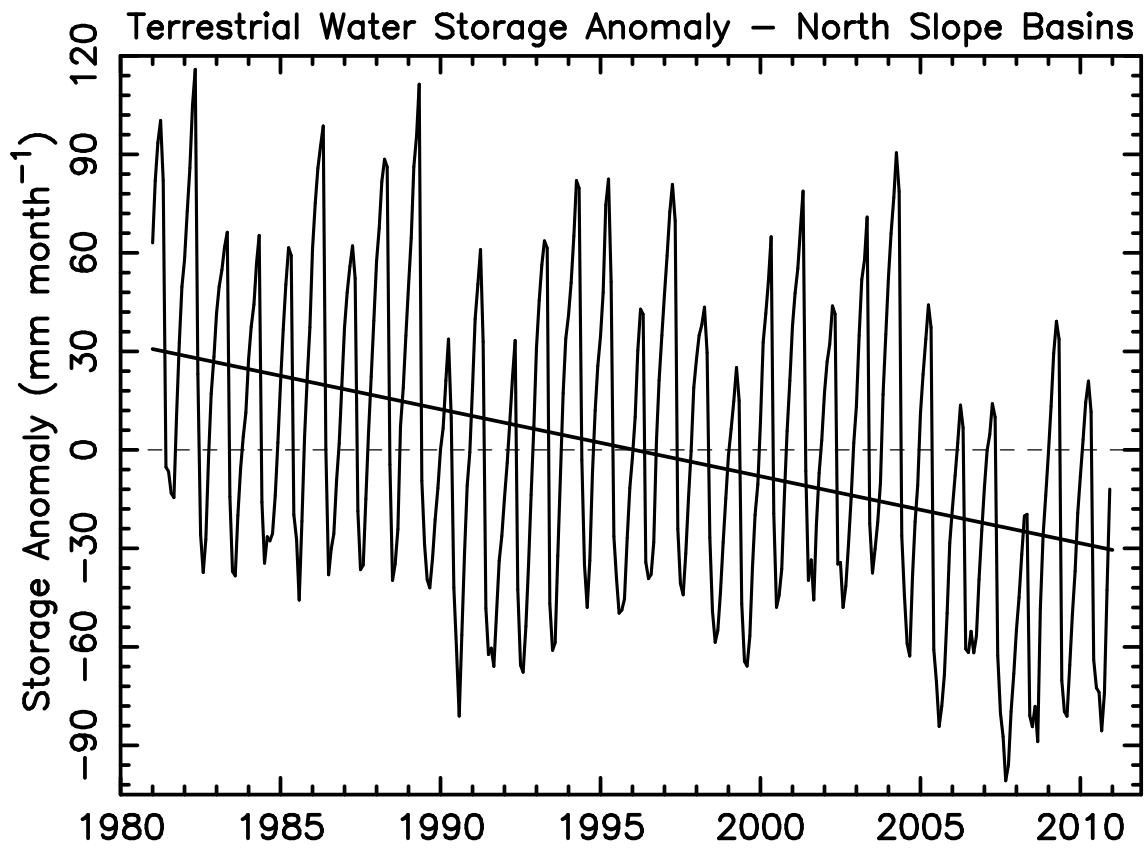


Figure 11: Terrestrial water storage (TWS) anomaly (mm month⁻¹) as an average across the North Slope drainage basin. Anomaly is with respect to the long-term average (1981–2010). In the [model-PWBM](#), TWS includes soil liquid water, ice, and snow storage. It does not include water stored in permanent water bodies such as ponds and lakes.

Table S1: [River basins ordered by size for the North Slope drainage region. Basins in the simulated topological network \(STN\) were defined on the 25×25 km² EASE-Grid \(Brodzik and Knowles, 2002\). Areas in km² based on extent in the STN of the full drainage basin info expressed to the respective river mouth at the coast. Names listed for rivers with areas greater than 4000 km². Unnamed rivers are numbered by size among all river basins in the pan-Arctic STN.](#)

Latitude	lonLongitude	Basin area	Name
70.3288	-151.0736	64095	Colville
70.6501	-154.3348	18851	GHAASBasin534 Ikpikpuk
70.2604	-148.1340	16338	GHAASBasin589 Sagavanirktok
70.9372	-156.1757	12568	Meade
70.3802	-148.6959	10054	Kuparuk
69.4239	-139.4672	6284	GHAASBasin1139 Firth
70.0799	-146.1292	5655	Canning
69.8753	-144.1624	5027	GHAASBasin1302 Hulahula
70.0150	-147.0306	4399	GHAASBasin1403 Shaviovik
68.5119	-135.8551	4399	GHAASBasin1453 Unnamed
70.8438	-155.5560	3770	GHAASBasin1659 Basin 1659
69.5061	-141.7360	3142	GHAASBasin1882 Basin 1882
68.6613	-137.1530	3142	GHAASBasin1896 Basin 1896
69.9243	-143.2594	2514	GHAASBasin1949 Basin 1949
69.7866	-142.7447	2514	GHAASBasin1966 Basin 1966
69.1231	-138.5215	2514	GHAASBasin2012 Basin 2012
68.6711	-136.2922	2514	GHAASBasin2041 Basin 2041
69.6471	-142.2369	2514	GHAASBasin2104 Basin 2104
68.8289	-136.7357	1885	GHAASBasin2279 Basin 2279
68.9706	-138.0587	1885	GHAASBasin2354 Basin 2354
70.1386	-147.5789	1885	GHAASBasin2463 Basin 2463
69.5720	-139.9503	1885	GHAASBasin2464 Basin 2464
68.6760	-135.4308	1885	GHAASBasin2466 Basin 2466
71.2383	-156.5290	1257	GHAASBasin3496 Basin 3496
70.9549	-154.6538	1257	GHAASBasin3497 Basin 3497
70.3011	-149.6013	1257	GHAASBasin3498 Basin 3498
69.9515	-145.5915	1257	GHAASBasin3500 Basin 3500
69.8212	-145.0607	1257	GHAASBasin3501 Basin 3501
69.2742	-138.9909	1257	GHAASBasin3503 Basin 3503
69.3244	-135.4441	1257	GHAASBasin3504 Basin 3504
70.8546	-152.5256	628	GHAASBasin4393 Basin 4393
70.4159	-150.1729	628	GHAASBasin4394 Basin 4394
69.5415	-140.8446	628	GHAASBasin4398 Basin 4398
69.0003	-135.4374	628	GHAASBasin4409 Basin 4409
68.8388	-135.0000	628	GHAASBasin4410 Basin 4410
69.3244	-134.5559	628	1 GHAASBasin4416 Basin 4416
69.4845	-134.1048	628	GHAASBasin4419 Basin 4419
71.1461	-155.8978	628	GHAASBasin6501 Basin 6501
70.4384	-151.6543	628	GHAASBasin6502 Basin 6502
70.0604	-143.7812	628	GHAASBasin6507 Basin 6507
68.8167	-137.6026	628	GHAASBasin6511 Basin 6511
69.1605	-135.8814	628	GHAASBasin6513 Basin 6513

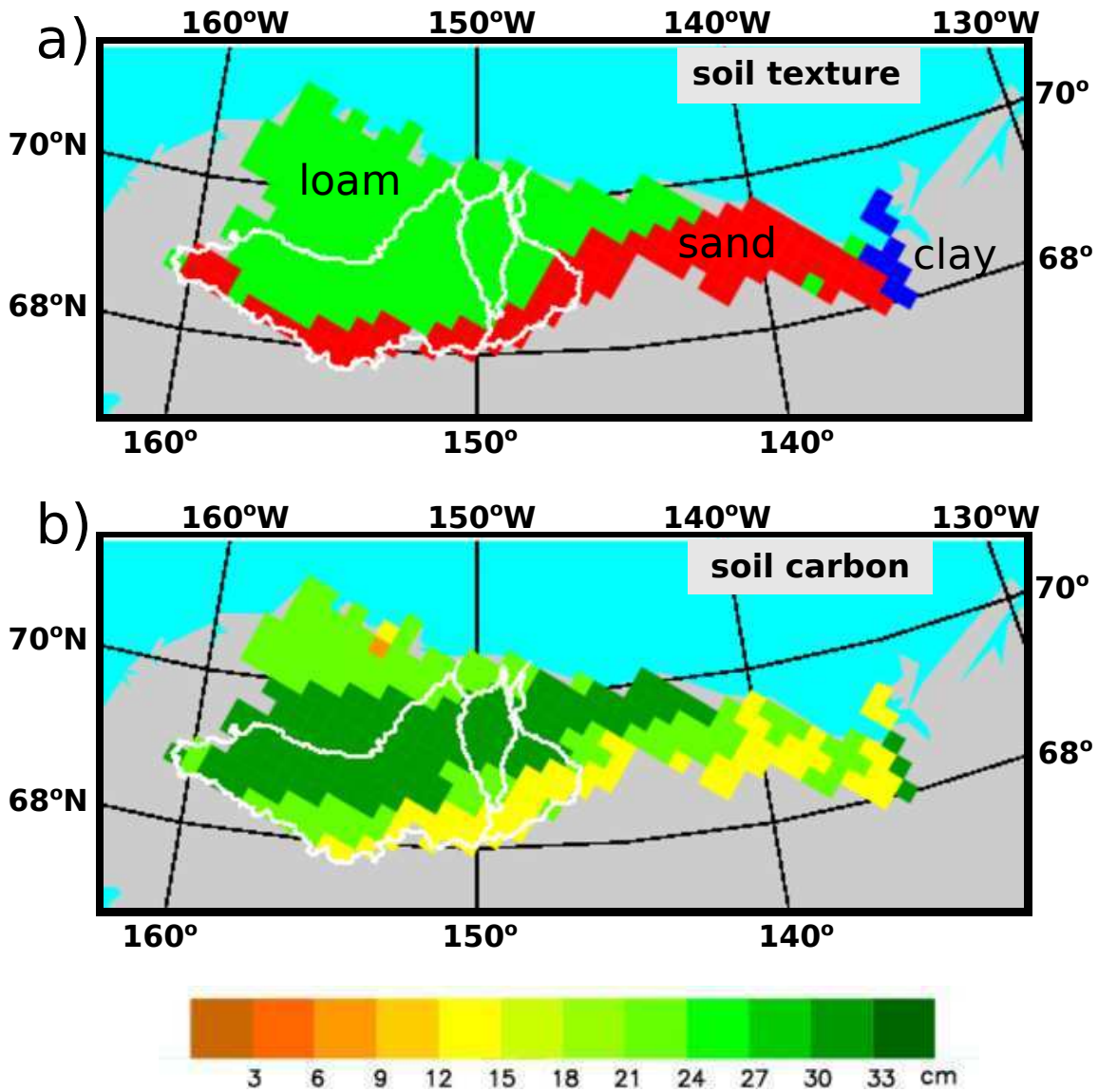


Figure S1: a) Soil texture classes and b) thickness of surface soil carbon layer used in model parameterizations. Soil [textures are drawn from the UNESCO Food and Agriculture Organization's Digital Soil Map of the World \(Food and Agriculture Organization/UNESCO, 1995\)](#). Soil carbon is taken from the [Northern Circumpolar Soil Carbon Database \(NCSCD\) \(Hugelius et al., 2014\)](#). Soil carbon thickness [derived from the NCSCD data and used in the PWBM](#) includes all soil layers for which some amount of carbon is present. Primarily mineral soil exists downward over the remainder of the soil column.

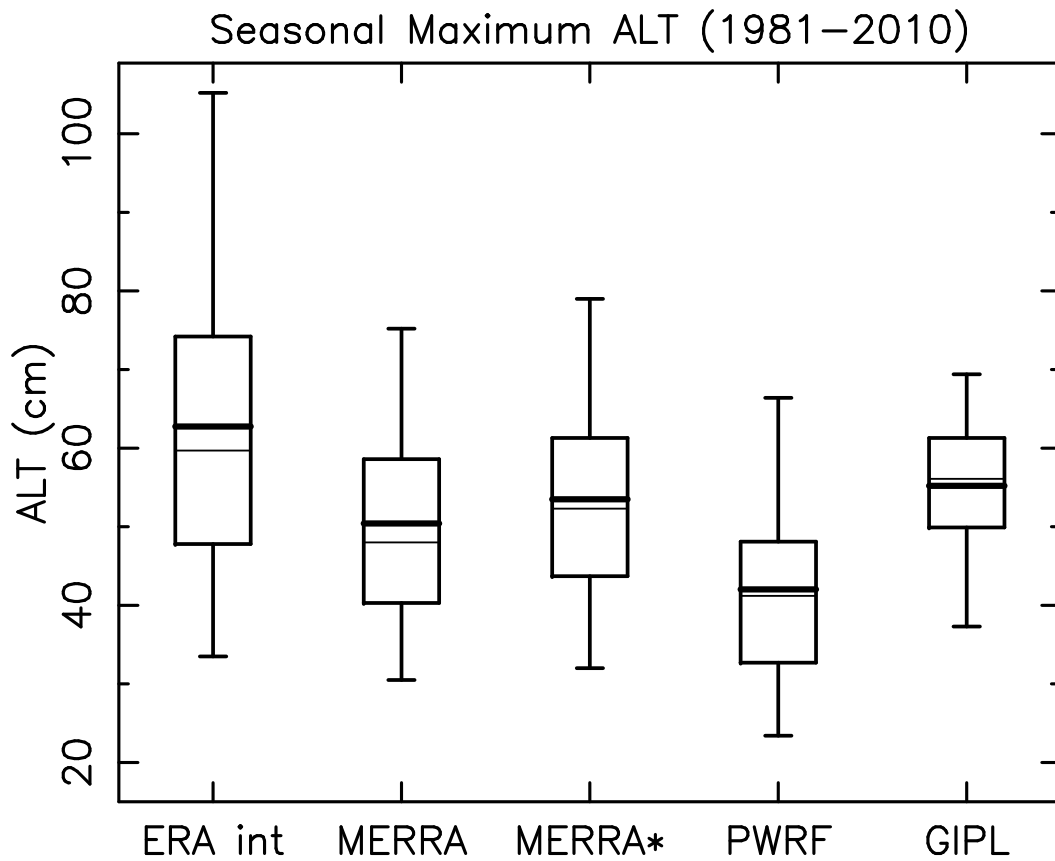


Figure S2: a) [Seasonal maximum ALT \(cm\) as an average over the period 1981–2010 from PWBM simulations and the GIPL model. Boxplots represent the 217 \(of 312\) PWBM domain grid cells for which GIPL ALT data are available. Boxplots were drawn from PWBM simulation using climate forcings from ERA interim, MERRA, MERRA with precipitation adjustment \(MERRA*\), and Polar WRF. Heavy line in each box is the distribution mean. Thin line is the distribution median. Boxes bracket the 25th and 75th percentiles. Whiskers show the 5th and 95th percentiles. From PWBM soil temperatures the seasonal maximum ALT is calculated as the depth to which the 0 °C penetrates each summer. Nicolsky et al. \(2017\) provide details on the GIPL ALT.](#)

Seasonal Maximum ALT

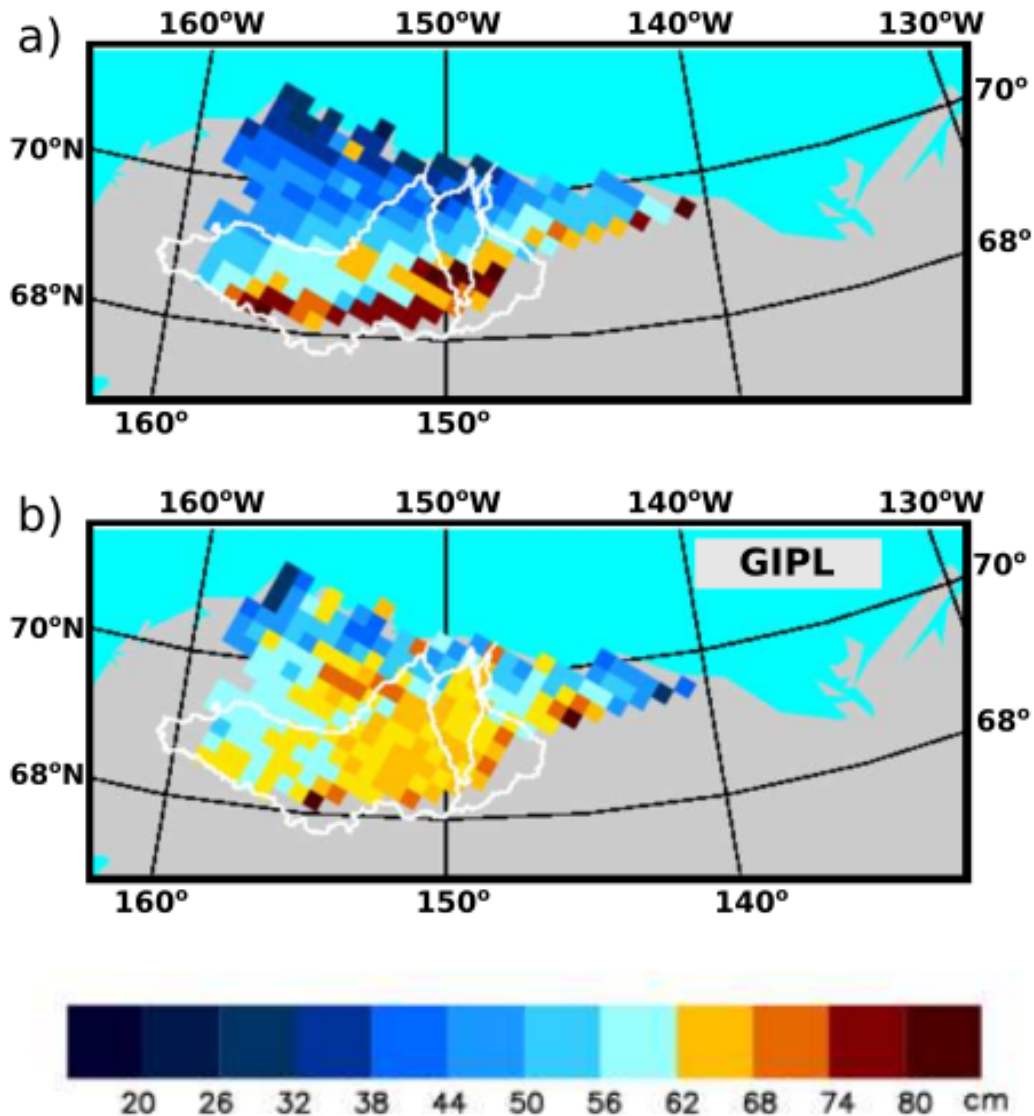


Figure S3: a) Seasonal maximum ALT (cm) as an average over the period 1981–2010 from a) PWBM with MERRA* forcing and b) GIPL. ~~Evaluations are made for the 217 (of 312) domain grid cells which have GIPL ALT data. For PWBM the seasonal maximum ALT is calculated as the depth to which the 0°C penetrates each summer. Nicolsky et al. (2017) provides details on the GIPL ALT.~~

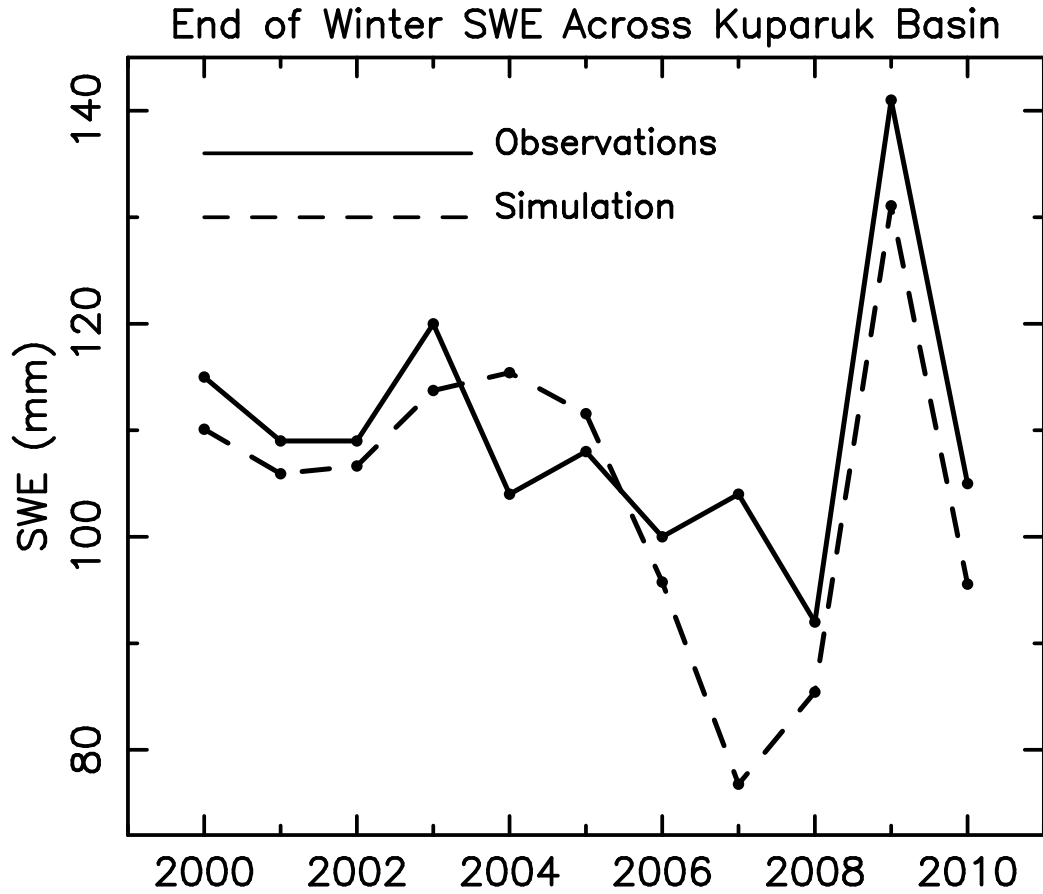


Figure S4: Observed and model simulated end of winter snow water equivalent (SWE, mm) for the Kuparuk River basin 2000–2010. Observed values represent an average of measurements made across the basin as described by Stuefer et al. (2013). Simulated end of season SWE is calculated as the average between 24 April and 7 May each year.

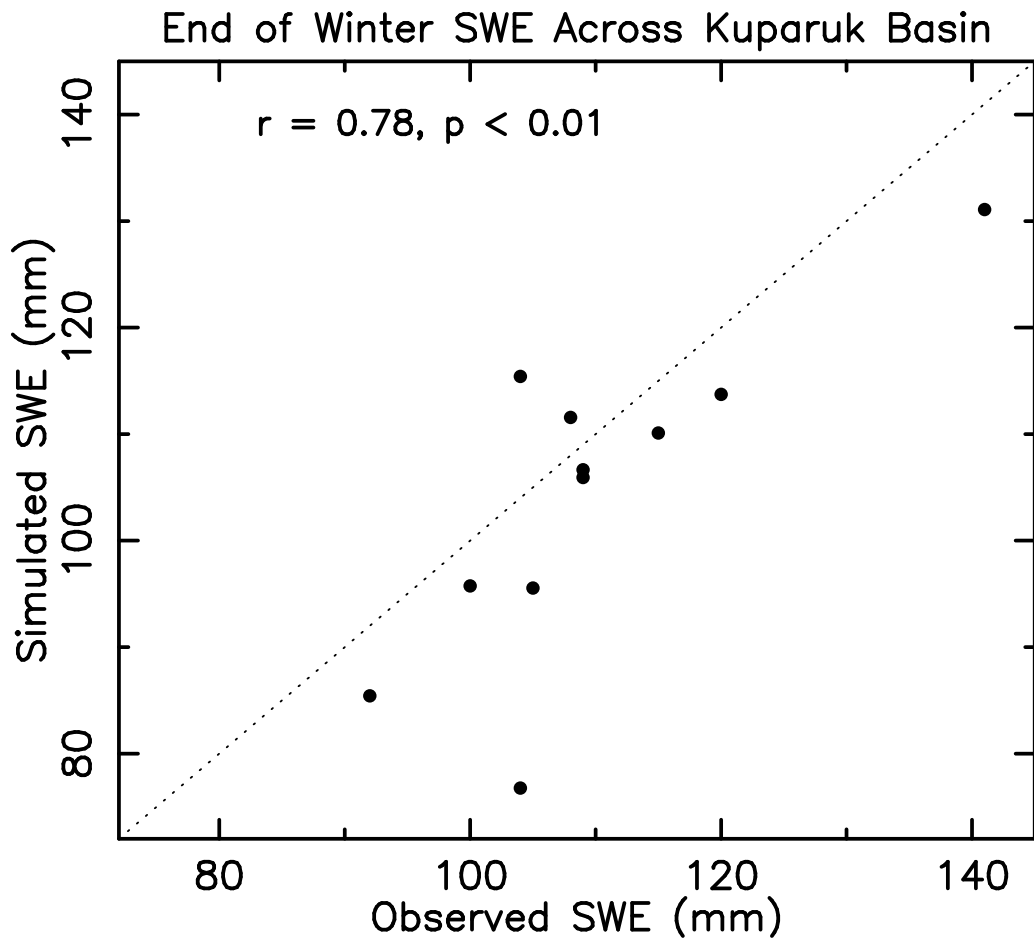


Figure S5: Observed and model simulated end of winter SWE (mm) for the Kuparuk Basin 2000–2010.

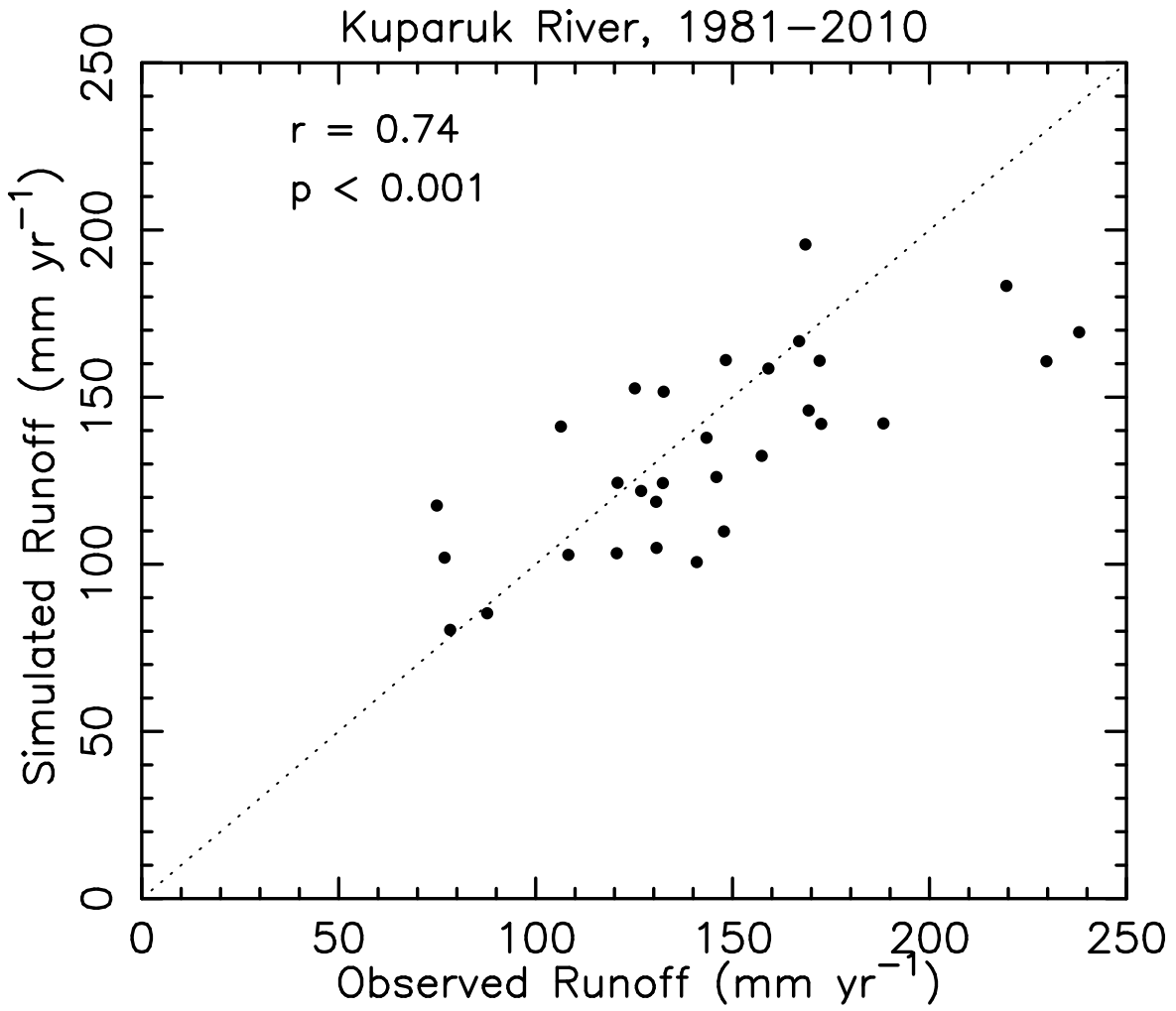


Figure S6: Simulated vs. observed annual total R (mm yr^{-1}) for the Kuparuk basin. Correlation coefficient (LLS) is $r = 0.73$ ($p < 0.001$).

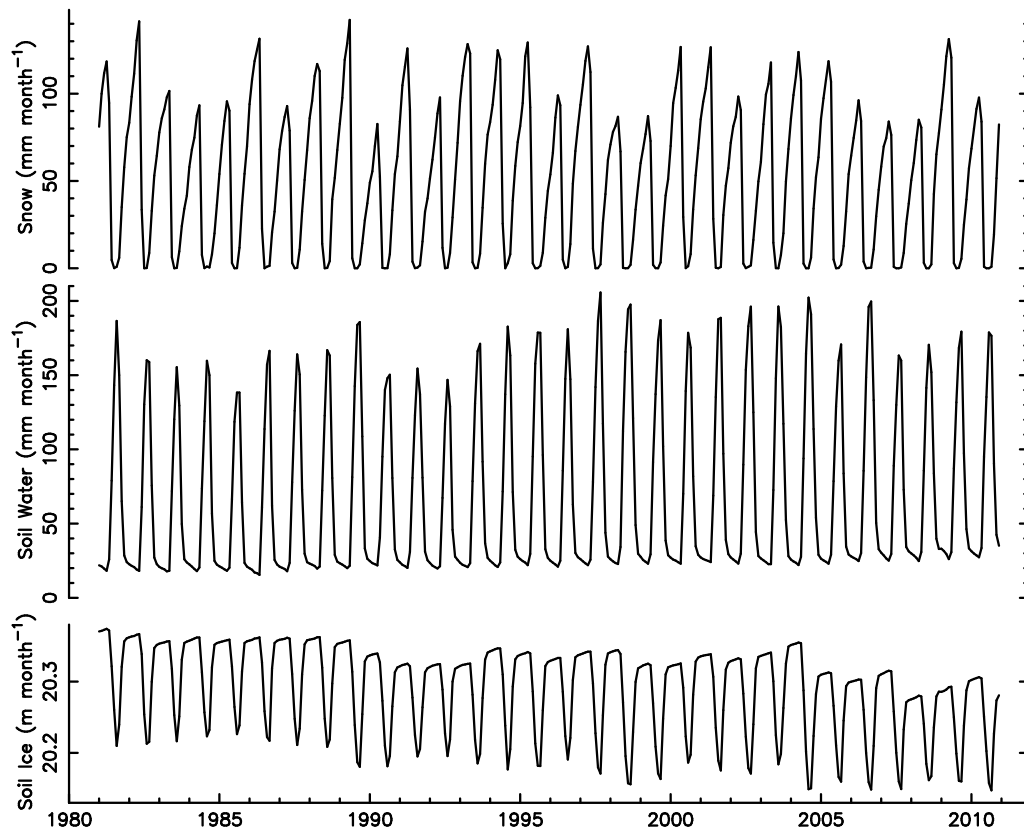


Figure S7: Monthly water storage for snow (solid and liquid portions, mm month⁻¹), soil water (mm month⁻¹), and soil ice (m month⁻¹) as an average across the North Slope drainage basin. Amounts are totaled over the full 60 m model soil column

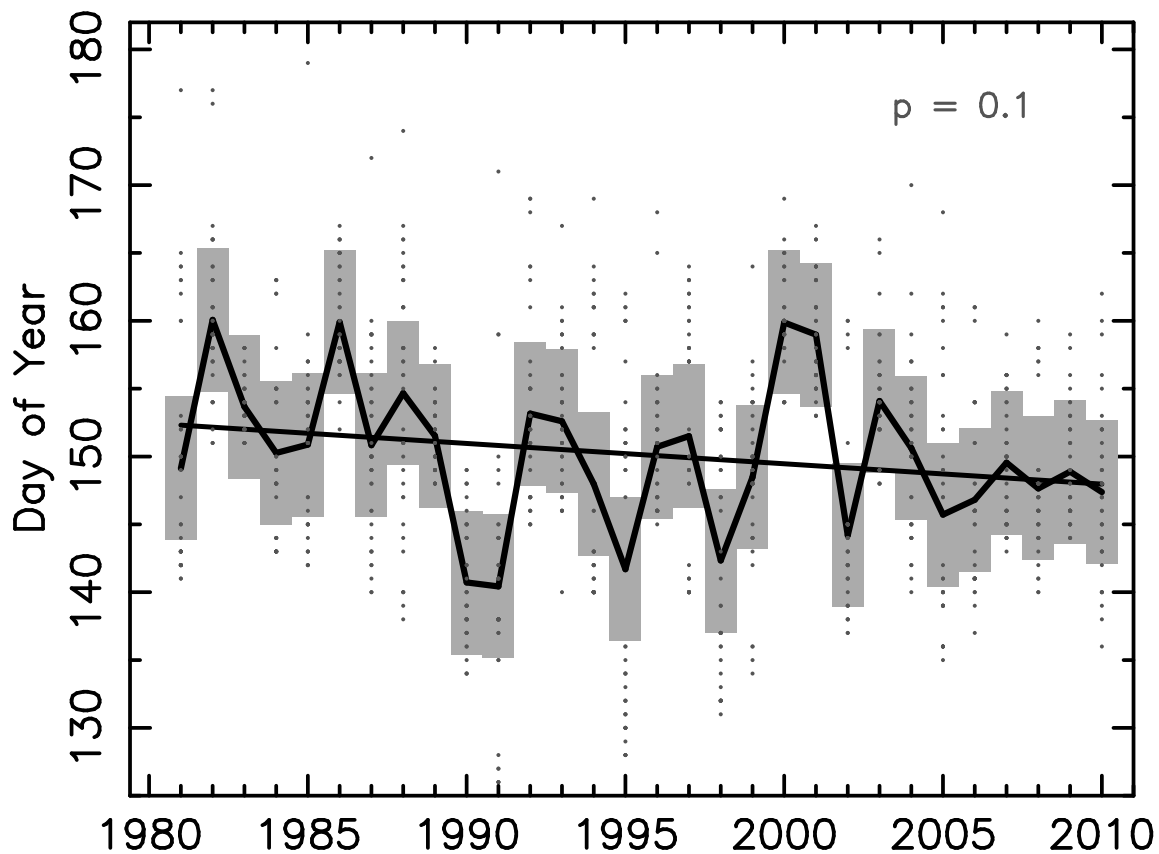


Figure S8: Date of maximum [river-daily Q](#) 1981–2010 for all 42 North Slope rivers. Gray bar shows the 1- σ range around the average date (solid line). Dots indicate the date for each [basin-river](#). Linear least squares trend shown. Significance of linear trend (GLM) is approximately $p = 0.1$